A derecho climatology (2004-2021) in the United States based on machine learning identification of bow echoes

Jianfeng Li[1, *], Andrew Geiss[1], Zhe Feng[1, *], L. Ruby Leung[1], Yun Qian[1], Wenjun Cui[2, 3]

[1]Atmospheric, Climate, and Earth Sciences Division, Pacific Northwest National Laboratory, Richland, Washington, USA

[2]Cooperative Institute for Severe and High-Impact Weather Research and Operations, University of Oklahoma, Norman, Oklahoma, USA

[3]National Severe Storms Laboratory, National Oceanic and Atmospheric Administration, Norman, Oklahoma, USA

*Correspondence to Jianfeng Li (jianfeng.li@pnnl.gov) and Zhe Feng (zhe.feng@pnnl.gov)

Abstract

Due to their persistent widespread severe winds, derechos pose significant threats to human safety and property, with impacts comparable to many tornadoes and hurricanes. Yet, automated detection of derechos remains challenging due to the absence of spatiotemporally continuous observations and the complex criteria employed to define the phenomenon. This study presents an objective derecho detection approach capable of automatically identify derechos in both observations and model results. The approach is grounded in a physically based definition of derechos and integrates three algorithms: (1) the Python Flexible Object Tracker (PyFLEXTRKR) algorithm to track mesoscale convective systems (MCSs), (2) a semantic segmentation convolutional neural network to identify bow echoes, and (3) a comprehensive classification algorithm to detect derechos within MCS lifecycles and distinguish derecho-producing from non-derecho-producing MCSs. Using this approach, we develop a novel high-resolution (4 km and hourly) observational dataset of derechos and accompanying derecho-producing MCSs over the United States east of the Rocky Mountains from 2004 to 2021. The dataset consists of two subsets based on different gust speed data sources and is analyzed to document the climatology of derechos in the United States. On average, 12-15 derechos are identified per year, aligning with previous estimations (~6-21 events annually). The spatial distribution and seasonal variation patterns are consistent with prior studies, showing peak occurrences in the Great Plains and Midwest during the warm season. Additionally, during the study period, derechos account for approximately 3.1% of measured damaging gusts (≥ 25.93 m s^{-1}) over the eastern United States. The dataset is publicly available at https://doi.org/10.5281/zenodo.14835362 (Li et al., 2025).

1 Introduction

35 A derecho is qualitatively defined as a widespread, long-lived straight-line windstorm associated

36 with a fast-moving mesoscale convective system (MCS), and the latter is named a derecho-producing

37 MCS (DMCS). Figure 1 shows two of the most destructive derechos and their accompanying DMCSs in

38 the United States: the June 2012 North American derecho and the August 2020 Midwest Derecho. Both

39 events lasted for over 10 hours, with apparent bow echoes and extensive damaging wind gusts ($\geq$ 25.93 m

40 s^{-1}).; https://www.weather.gov/mlb/wind_threat; last access: 8 April 2025). Due to the persistent

41 widespread damaging gusts, derechos can severely damage property and threaten human lives, as

42 exemplified by the extensive power outages and more than ten fatalities caused by the two derechos.

43 Ashley and Mote (2005) demonstrated that derechos could be as hazardous as and were comparable in

44 impact to most hurricanes and tornadoes in the United States between 1986 and 2003.
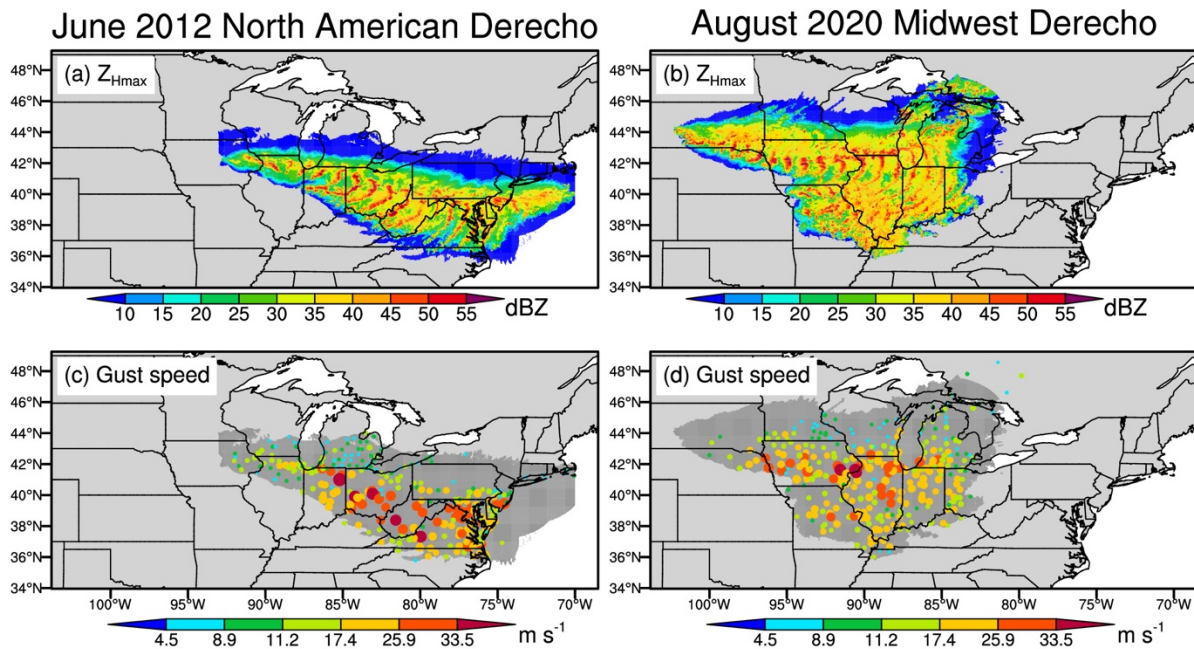
46 Figure 1. Spatial evolutions of the (a, b) composite (column-maximum) radar reflectivity (Z_{Hmax}) signatures
47 and (c, d) surface gust speeds (colored dots) of two DMCSs. The first column is for the DMCS associated with
48 the June 2012 North American derecho, which occurred on 29-30 June 2012, and the right column is the
49 August 2020 Midwest derecho accompanying DMCS, which occurred on 10-11 August 2020. Due to
50 spatiotemporal overlapping, multiple Z_{Hmax} and gust speeds may exist for a given grid cell or weather station,
51 in which case only the corresponding maximums are shown in the figure. In (c) and (d), the dark gray shading

52 refers to DMCS cold cloud coverage. The dot sizes in (c) and (d) are proportional to the gust speed
53 magnitudes. Notably, gust speed in (c) and (d) is based on the hourly maximum gust speed ($gust_{hourly\_max}$),
54 which is the largest gust speed within one hour if multiple gust speed measurements are available.

55   A reliable derecho dataset is foundational for understanding the underlying physical mechanism of

56 derecho initiation and development and their socioeconomic impacts. Johns and Hirt (1987) developed

57 the first derecho climatology in the warm seasons of 1980-1983 in the United States by quantitatively

58 defining a derecho as a family of downburst clusters produced by an extratropical MCS. Specifically, they

59 required a derecho to satisfy the following six criteria.

60   1) There must be a concentrated area of reports with wind damage or convective gusts > 25.7 m

61   s^{-1}, and the major axis length of the area must be at least 400 km.

62   2) Those wind damage or convective gust reports must show a pattern of chronological

63   progression, either as a singular swath or a series of swaths.

64   3) The concentrated area must have at least three reports of either F1 damage (32.7-50.3 m s^{-1})

65   (Fujita, 1971) or convective gust of at least 33.4 m s^{-1} separated by ≥ 64 km.

66   4) At most 3 hours can elapse between successive reports of wind damage or gust > 25.7 m s^{-1}.

67   5) The associated convective system must have temporal and spatial continuity in surface

68   pressure and wind fields.

69   6) If multiple swaths of wind damage or gust reports > 25.7 m s^{-1} exist, they must be from the

70   same MCS event.

71   Since then, several other studies have developed derecho climatologies during other periods using

72 slightly different criteria (Bentley and Mote, 1998; Evans and Doswell, 2001; Bentley and Sparks, 2003;

73 Coniglio and Stensrud, 2004; Guastini and Bosart, 2016). For example, Bentley and Mote (1998)

74 removed the third requirement and reduced the elapsed time in the fourth condition from no more than 3

75 hours to no more than 2 hours in their derecho climatology from 1986 to 1996. In Coniglio and Stensrud

76   (2004), the elapsed time was further changed to no more than 2.5 hours, and the gust reports of at least 33

77   m s^{-1} were used to separate derechos of different intensities.

78   Although the aforementioned derecho datasets were generated using different criteria and during

79   different periods (Johns and Hirt, 1987; Bentley and Mote, 1998; Evans and Doswell, 2001; Bentley and

80   Sparks, 2003; Coniglio and Stensrud, 2004; Guastini and Bosart, 2016), they showed many similar

81   derecho climatological characteristics in the United States. For example, derechos occur more frequently

82   in the warm than cold seasons; the Great Plains, Midwest, and Ohio Valley are regions most favorable for

83   derecho development, and few derechos occur in the eastern and western coastal areas. Considering the

84   inconsistent thresholds used in the above studies and the lack of physical mechanisms in their derecho

85   definitions, Corfidi et al. (2016) proposed a stricter and more physically based derecho definition, which

86   required the existence of sustained bow echoes with mesoscale vortices or rear-inflow jets and a nearly

87   continuous wind damage swath of at least 100 km wide along most of its extent and 650 km long. In

88   addition, the wind damage must occur after the convective system was organized into a cold-pool-driven

89   forward-propagating MCS. Most derechos satisfying this definition would be classified as "progressive"

90   but not "serial." A serial derecho typically originates in strongly forced environments and develops from a

91   mature squall line with multiple embedded bow echoes. In contrast, progressive derechos generally

92   originate from small convective clusters that grow upscale into large organized forward-propagating

93   MCSs in synoptic environments with weak forcing (Squitieri et al., 2023)(Squitieri et al., 2023; Corfidi et

94   al., 2016).

95   It is difficult to develop a derecho climatology using the definition proposed by Corfidi et al. (2016)

96   with current operational measurements, as it involves the identification of bow echoes, rear-inflow jets,

97   and cold pools. However, rear-inflow jets and cold pools are generally associated with bow echoes

98   (Weisman, 1993; Adams-Selin and Johnson, 2010). Once long-lived bow echoes are found in an MCS,

99   we can expect the simultaneous existence of rear-inflow jets and cold pools. Nevertheless, identifying

100   bow echoes, a feature typically identified visually from radar observations, is still challenging for large

101 volumes of data, such as the 30+ year National Oceanic and Atmospheric Administration (NOAA) Next

102 Generation Weather Radar (NEXRAD) archive consisting of 159 radars. The manual examination is time-

103 consuming and sensitive to subjective biases. ~~This~~The present study applies a semantic segmentation

104 convolutional neural network (CNN) to detect bow echoes automatically from two-dimensional

105 composite (column-maximum) reflectivity (Z_{Hmax}) data in the United States, which are then combined

106 with an MCS tracking dataset and surface gust speeds to identify derechos using criteria adjusted from

107 Corfidi et al. (2016). After manual examination and validation, we produce a high-resolution ~~(4 km and~~

108 ~~hourly)~~ observational derecho and DMCS dataset in the United States east of the Rocky Mountains from

109 2004 to 2021~~.~~ at 4 km spatial and hourly temporal resolution. The dataset comprises two subsets based on

110 different gust speed data sources: one uses gust speed measurements from the global hourly Integrated

111 Surface Database (ISD) (NOAA/NCEI, 2001), and the other exploits gust speed reports from the NOAA's

112 Storm Events Database (SED). As the first derecho climatology that utilizes a machine learning technique

113 following physically based criteria and covers the recent decades, the dataset provides a reference for

114 future derecho ~~studies and can be used to investigate the underlying mechanisms for~~ research, enabling

115 investigation of derecho initiation and development mechanisms, the climatological impacts of derechos

116 on hazardous weather, and ~~the~~their potential damage ~~of derechos~~ to infrastructure and ~~human~~ property.

117   The remainder of the paper is organized as follows. Section 2 introduces the MCS and gust speed

118 datasets used to generate the derecho dataset. Section 3 describes the machine learning (i.e., semantic

119 segmentation CNN) methodology to detect bow echoes, including sampling, training, and evaluation.

120 Section 4 explains our derecho identification criteria in detail. Section 5 evaluates our derecho dataset

121 through cross-validation of the two subsets (ISD-based vs. SED-based) and compare them with previous

122 derecho estimations and the observational data from the NOAA Storm Prediction Center (SPC) in 2004

123 and 2005. Section 6 analyzes the derecho climatological characteristics. Section 7 shows how to access

124 our derecho dataset, and the study is summarized in Section 8.

2 Source datasets

2.1 MCS dataset

Since previous MCS datasets only cover the period from 2004 to 2017 (Li et al., 2021; Feng et al., 2019), we use an updated version of the Python FLEXible Object TRacKeR (PyFLEXTRKR) software (Feng et al., 2023), which exploits collocated radar signatures, satellite infrared brightness temperature, and precipitation to identify robust MCS events (Feng et al., 2019), to produce an updated 4-km and hourly MCS dataset in the United States east of the Rocky Mountains from 2004 to 2021 (Feng, 2024). Several hourly source datasets are used in the generation of the MCS dataset, including the National Centers for Environmental Prediction (NCEP)/the Climate Prediction Center (CPP) L3 4 km Global Merged IR V1 brightness temperature dataset (Janowiak et al., 2017), the three-dimensional Gridded NEXRAD Radar (GridRad) dataset (Bowman and Homeyer, 2017), the NCEP Stage IV precipitation dataset (CDIACS/EOL/NCAR/UCAR and CPC/NCEP/NWS/NOAA, 2000), and melting level heights derived from ERA5 (European Centre for Medium-Range Weather Forecasts (ECMWF) Reanalysis v5) (Hersbach et al., 2023). The MCS definition criteria are almost the same as those in Feng et al. (2019), such as cold cloud shield (CCS) area > 60,000 km^2, precipitation feature (PF, which is a continuous convective or stratiform area with surface rain rate > 2 mm h^{-1}) major axis length > 100 km, the existence of 45-dBZ convective echoes, etc., except that the duration requirement is lowered to include those convective systems lasting for just 6 hours. This adjustment allows us to capture slightly shorter-lived MCSs that may produce intense wind gusts but are missed in the previous MCS datasets. Convective and stratiform radar echo classification in PyFLEXTRKR follows the Storm Labeling in 3D (SL3D) algorithm (Starzec et al., 2017), which uses horizontal texture and vertical structure of radar reflectivity from the GridRad product. Notably, the GridRad data are available each month from 2004 to 2017 but only between April and August from 2018 to 2021. Since most derechos occur in the warm season (Ashley and Mote, 2005; Coniglio and Stensrud, 2004), missing the cold months between 2018 and 2021

149   does not affect our derecho climatological analyses in Section 6. For brevity, we do not mention the

150   missing cold months between 2018 and 2021 in the following sections unless stated otherwise.

2.2 Surface gust speed datasets

2.2.1 ISD gust speed measurements

153   The ISD is developed by the NOAA National Centers for Environmental Information (NCEI) in

154   collaboration with several other institutions. ISD compiles global hourly and synoptic surface

155   observations from numerous sources (e.g., the Automated Surface Observing System and the Automated

156   Weather Observing System) into a single common format and data model. Besides internal quality control

157   procedures conducted by the source datasets, ISD applies additional quality control algorithms to process

158   each observation through a series of validity checks, extreme value checks, and internal and external

159   continuity checks (Smith et al., 2011). This study uses ISD gust speed measurements passing all quality

160   control checks (NOAA/NCEI, 2018). Notably, there may be multiple measurements at different times

161   within one hour for some stations. To keep the sampling consistency across different datasets used in the

162   derecho identification, we calculate $gust_{hourly\_max}$, which is the largest gust speed of all available

163   measurements within one hour, for each observational site, unless stated otherwise. A total of 4,260

164   observational sites provide gust speed measurements between 2004 and 2021 in the study domain, of

165   which 3,954 are over land, and the rest are over the ocean or lakes (Figure S1). We have excluded one

166   observational site (ISD station ID: 726130-14755) in the northeastern United States, which has an

167   unrealistic number of damaging gust measurements (more than 1,000 hours), inconsistent with the

168   surrounding sites. We note that although we only use measurements passing all the available quality

169   control checks, spatial quality control is missing in the ISD (Smith et al., 2011). Figure S2a shows that

170   some sites in the eastern United States have apparently more damaging gust occurrences than their

171   surrounding sites, but the occurrence frequencies are less than those stations around the Rocky

172   Mountains. We do not have enough evidence to exclude them from the study. The quality of the ISD gust

173 speed measurements will undoubtedly be a source of uncertainty for our derecho dataset. In addition, only

174 420 ISD sites have continuous gust measurements from 2004 to 2021, while the rest have gust

175 measurements only during part of the study period. The availability of ISD observational sites is another

176 source of uncertainty when identifying derechos.

177 *2.2.2 SED gust speed reports*

178 The SED is also maintained by the NOAA NCEI and serves as NOAA's official publication

179 documenting storms and other significant weather phenomena that are intense enough to cause

180 socioeconomic damage (NOAA/NCEI, 2025). The National Weather Service (NWS) compiles storm data

181 from a wide range of sources beyond meteorological weather stations and submits them to NCEI. These

182 sources include, but are not limited to, local and federal law enforcement agencies, government officials,

183 Skywarn spotters, NWS damage surveys, the insurance industry, newspaper clipping services, media

184 reports, private companies, and individuals. While the NWS strives to use the best available information,

185 some data in the SED remain unverified due to time and resource constraints. Consequently, the dataset

186 suffers from inaccuracies, inconsistencies, and gaps (Santos, 2016). For example, Ardon-Dryer et al.

187 (2023) found that half of the "dust storms" recorded in the SED had visibilities larger than 1 km,

188 indicating misclassification, while many actual dust storms with visibilities of ≤ 1 km were missing from

189 the dataset. These issues were attributed in part to the diverse sources contributing to the SED and the

190 lack of systematic verification and consistency checks. Considering these limitations, particularly the fact

191 that many strong (≥ 17.43 m s^{-1}) and damaging gust reports in the SED are estimated rather than

192 measured, the derecho and DMCS dataset developed from SED in this study is published as a supplement

193 to the dataset derived from the ISD.

194 From the SED, we extract measured and estimated gusts, along with their corresponding locations

195 and timestamps, for the period from 2004 to 2021. The raw SED files are available at

196 https://www.ncei.noaa.gov/pub/data/swdi/stormevents/csvfiles/ (NOAA/NCEI, 2025). If a gust report is

197 recorded as a segment, containing both a start and end location with respective timestamps, we process it

198 as two independent reports: one at the start location and time and another at the end location and time.

199 Although the accuracy of the SED gust speeds is not guaranteed, the database provides significantly more

200 strong and damaging gust reports than the ISD due to its inclusion of estimated gusts from various

201 sources. Approximately 82% of SED gust reports from 2004 to 2021 are estimated, while only 18% are

202 measured. However, it is important to note that not all measured strong or damaging gusts are captured in

203 the SED. Given the distinct limitations of both the ISD and SED datasets, we apply different thresholds

204 criteria for derecho detection depending on the dataset used. These criteria are described in detail in

205 Section 4.

3 Machine learning identification of bow echoes

206

207 A bow echo is a bow-shaped pattern with high reflectivity values on a radar image, but its vague

208 definition makes it hard to identify them extensively and efficiently using traditional methods. Instead, we

209 train a semantic segmentation CNN to identify bow echoes automatically from two-dimensional Z_{Hmax}

210 images by performing pixel-level labeling of the bow echo extent. Compared to the manual examination

211 of radar images, machine learning can save a tremendous amount of time and eliminate subjective bias.

3.1 Bow Echo Samples

212

213 *3.1.1 Initial manual sampling*

214 Our initial bow echo samples are generated based on the named derechos on Wikipedia

215 (https://en.wikipedia.org/wiki/List_of_derecho_events; last access: 19 March 2023), corresponding to 54

216 accompanying DMCSs in the MCS dataset. We manually label times with apparent bow echoes through

217 visual inspection of hourly Z_{Hmax} associated with the tracked DMCSs. Each positive sample is a 384 ×

218 384-pixel (~1536 km × 1536 km) Z_{Hmax} image centered at the corresponding DMCS with a bow echo

219   embedded (Figure 2). The number of bow echo samples varies among different DMCSs, and 566 positive

220   samples (with bow echoes) are obtained in total. 5400 negative samples (generally without bow echoes)

221   are also randomly selected from the entire 18 years of radar reflectivity data embedded in the MCS

222   dataset.
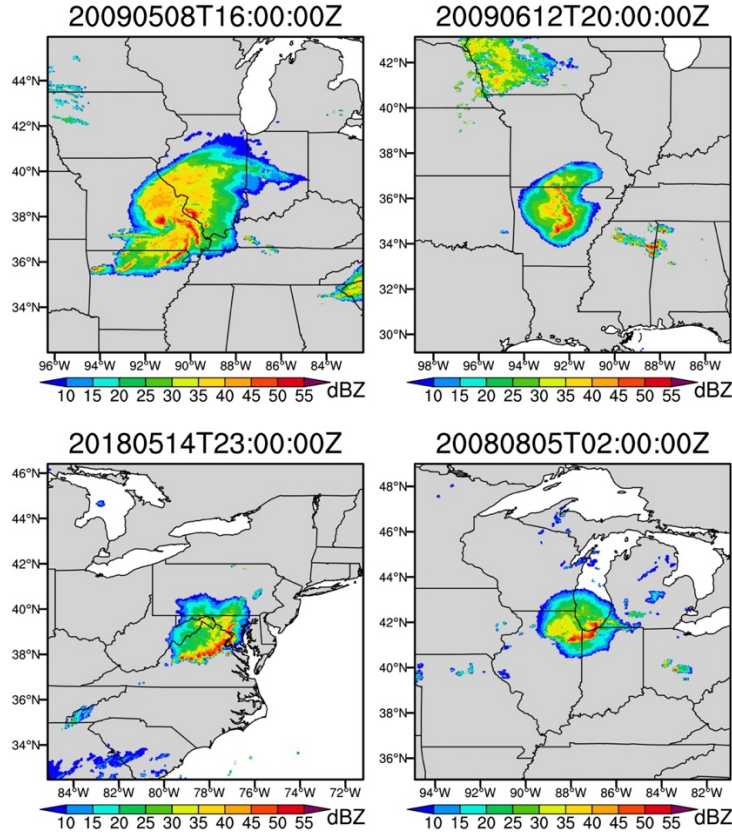
223
224   Figure 2. Four examples of bow echoes from the named derecho accompanying DMCSs. The color shading is
225   for Z_{Hmax}. The subplot titles indicate the bow echo timings.occurrence times. For example,
226   20130613T04:00:00Z represents 4:00 UTC on 13 June 2013.

227   *3.1.2 CNN-based selection of additional bow echo samples*

228   Our initial attempt at developing an automated bow echo detection scheme is to train a classifier

229   CNN — "Dense Net" (Huang et al., 2019) that ingests 384×384-pixel single-channel Z_{Hmax} images and

230   outputs a single classification indicating the presence of a bow echo. Dense Nets are notable for their

231   large number of skip connections (which create multiple paths for data to flow through the network

232   without passing through every layer), and they can achieve comparable performance to very large

233   classifier CNNs with only a fraction of the trainable parameters. Unfortunately, our manual inspection

234   finds that a Dense Net trained on the aforementioned initial samples has a very high false positive rate

235   when applied to the full radar dataset. Although this Dense Net is unsuitable for deployment, the

236   collection of new positive samples it successfully identifies allows us to supplement the list of known

237   bow echoes and develop a more diverse training set for the following segmentation model.

238   *3.1.3 Pseudo-labeling*

239   By combining the initial samples and the manually selected true positives from the low-quality

240   Dense Net model, we build a semantic segmentation training dataset of 500 unique bow echo snapshots

241   and corresponding hand-drawn bow echo masks. While 500 positive samples are relatively small for a

242   deep learning application, these samples have higher diversity than the initial bow echoes generated from

243   the named derechos on Wikipedia because they are drawn from ~~more distinct~~a broader range of events,

244   and, in general, semantic segmentation CNNs can be successfully trained with far fewer samples than

245   image classification CNNs (Bardis et al., 2020).

246   A relatively low-skill version of the semantic segmentation CNN is trained using the 500 hand-

247   labeled radar images and then applied to the entire Z_{Hmax} dataset. We manually review the bow echo

248   masks produced by this segmentation model and add some of the high-quality masks to a new training

249   dataset. We also collect some of its false positive masks as new negative samples in the new training

250   dataset. This is a semi-supervised learning approach known as "pseudo-labeling" or "bootstrapping" (Van

251   Engelen and Hoos, 2020; Ouali et al., 2020) and is commonly applied to semantic segmentation problems

252   because of the high expense of hand-drawn labels (Peláez-Vegas et al., 2023). The pseudo-labels and

253   hand-labels are combined into a final training dataset with 3677 samples, including 1699 bow echoes and

254   1978 negative samples, which is used to train the much more skillful semantic segmentation model in

255   Section 3.2.

256 *3.1.4 Data augmentation*

257   To combat the limited training data further, we use several data augmentation strategies when

258 constructing training batches. During training, positive and negative samples are selected with equal

259 probability, and a batch size of 8 is used. First, random salt and pepper noise is added to 10% of the pixels

260 in each sample with a probability of 0.1. (i.e., it has a probability of 0.1 to add random noise to a pixel).

261 Second, weak random Gaussian noise with a standard deviation of 5 dBZ is added to all the pixels in each

262 sample with a probability of 0.1. Third, samples are flipped in up-down and left-right directions, each

263 with a likelihood of 0.5. Fourth, samples are rotated by 0, 90, 180, or 270 degrees, each with a probability

264 of 0.25. Fifth, samples are randomly shifted vertically and horizontally by -5 to 5 pixels. Sixth, the

265 brightness of the sample image is adjusted by a random factor of -0.6 to +0.2, and the image contrast is

266 randomly adjusted by -0.2 to 0.2. Seventh, the binary target bow echo masks are multiplied by 0.9, and

267 random noise drawn from a uniform distribution between 0 and 0.1 is added. This is known as "soft

268 labels." Lastly, both positive and negative samples are blended with randomly selected negative samples

269 by taking the pixel-wise maximum reflectivity values of the two samples with a 0.5 likelihood. This last

270 data augmentation is unusual but works well in our application because a) reflectivity features typically

271 occupy only a fraction of the sample area, with most pixels being echo-free and b) bow echoes are high-

272 reflectivity features. When the last data augmentation is applied to a positive sample, the resulting image

273 will typically still contain a bow echo that matches the target mask well.

274 ## 3.2 Training of U-Net 3+ CNN

275   Our final semantic segmentation CNN model (Figure 3) uses the U-Net 3+ architecture (Huang et

276 al., 2020). U-Net 3+ is a modern variant of the U-Net architecture (Ronneberger et al., 2015) and differs

277 from the U-Net primarily in the addition of many more skip connections and its multi-resolution loss,

278 which computes loss on rescaled classification masks generated from feature representations at various

279 model levels.

280   U-Net models were originally developed for the segmentation of biomedical imagery but have been

281   applied to image segmentation problems in other fields and are broadly useful for any image-to-image

282   mapping tasks where the input and target data are the same (or similar) size and shape and merging multi-

283   resolution information from the input data is important. U-Net CNNs have been applied to a myriad of

284   problems in the atmospheric sciences, such as segmentation (Galea et al., 2024; Kumler-Bonfanti et al.,

285   2020), super resolution (Geiss and Hardin, 2020; White et al., 2024), physics parameterization

286   (Lagerquist et al., 2021), downscaling (Sha et al., 2020), and weather forecasting (Weyn et al., 2021).

287   Perhaps most closely related to this study is Mounier et al. (2022), who used a U-Net to detect bow

288   echoes in simulated radar reflectivity images from a forecast model. A U-Net is an appropriate choice for

289   the segmentation of bow echoes because merging multi-resolution information is crucial for identifying

290   the feature. For example, bow echoes have high reflectivity at the pixel scale, strong reflectivity gradients

291   in the transverse direction at the mid-scale (tens of pixels), and the characteristic bow shape at the large

292   scale (hundreds of pixels).
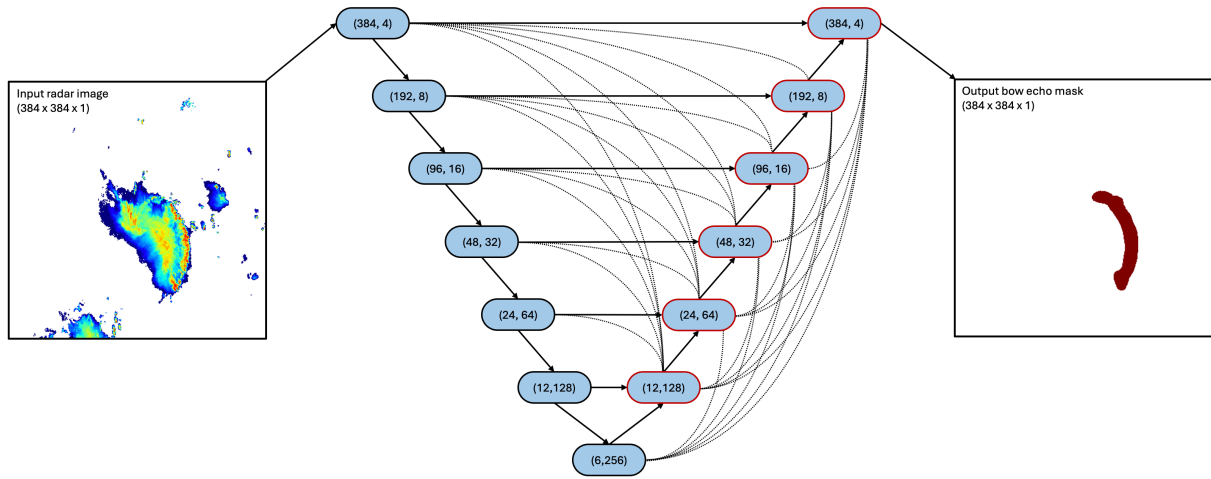
293
294   Figure 3. A diagram of our semantic segmentation CNN architecture. The CNN inputs a 384×384-pixel radar
295   image (Z_{Hmax} scaled to 0-255) and outputs a bow echo mask of the same size. The blue ovals represent 3×3
296   convolutional layers, each followed by a batch normalization layer and a leaky rectified linear unit (ReLU)
297   activation function. The first number in each blue oval indicates the spatial size (for both the width and height)
298   of the output tensor, and the second represents the number of output channels. The solid arrows indicate
299   connections in a standard U-Net architecture, with the downward arrows corresponding to 2×2 max-pooling
300   and the upward arrows corresponding to 2×2 bilinear upsampling operations. The dashed lines represent the
301   skip connections introduced in the U-Net 3+ architecture. These skip connections use max-pooling for spatial

302   downsampling and bilinear interpolation for upsampling, followed by a 16-channel 3×3 convolutional layer
303   with a linear activation. Layers with multiple inputs use channel-wise concatenation to combine those inputs.
304   During training, the output tensors from the layers in the upsampling branch (blue ovals with red boundaries)
305   are scaled to the output spatial resolution and passed through a 1-channel 1×1 convolutional layer with sigmoid
306   activation. Training loss is computed on all 6 of the resulting masks. At inference time, only the mask
307   outputted from the upper-rightmost layer is used.

308   Our U-Net 3+ CNN ingests 384×384-pixel Z_{Hmax} images where Z_{Hmax} have been clipped to a 0-50

309   dBZ range and then linearly mapped to a range of 0-255. It is trained using binary cross entropy loss

310   (Bishop, 2006) on masks generated from its 384, 192, 96, 48, 24, and 12-pixel resolution feature

311   representations (Huang et al., 2020), though only the full-resolution (384×384-pixel) output mask is used

312   at inference time. A detailed diagram of the model architecture is shown in Figure 3. Notably, although

313   the model is trained using 384×384-pixel samples, it is a fully convolutional model and can process inputs

314   of variable sizes.

315   We use the Adam optimizer (Kingma and Ba, 2014) with the Keras default settings (Ketkar, 2017)

316   and an initial learning rate of 0.001 for training. The U-Net 3+ CNN is first trained for 60 epochs

317   composed of 1000 randomly generated training batches of 8 samples each. Then, we decrease the learning

318   rate to 0.0001 and train the CNN for an additional 20 epochs. The training duration is determined by

319   performing an initial 5 rounds of training with 5-fold cross-validation and approximating the epoch

320   numbers to reduce the learning rate and stop training when the mean intersection over union metric

321   plateaus for the validation set. Instead of random shuffling, the validation sets are separated from the

322   training dataset in temporally contiguous chunks to avoid any overlap because, sometimes, multiple

323   samples may be drawn from different times of the same convective system.

3.3 Evaluation of the Semantic Segmentation CNN

325   We apply the trained U-Net 3+ CNN to the entire Z_{Hmax} dataset and obtain potential bow echo masks

326   over the United States between 2004 and 2021 (Figure 4). As a final post-processing step, we ignore

327   "bow echo" masks with less than 20 pixels (~320 km^2), which are too small to be classified as bow

328   echoes.
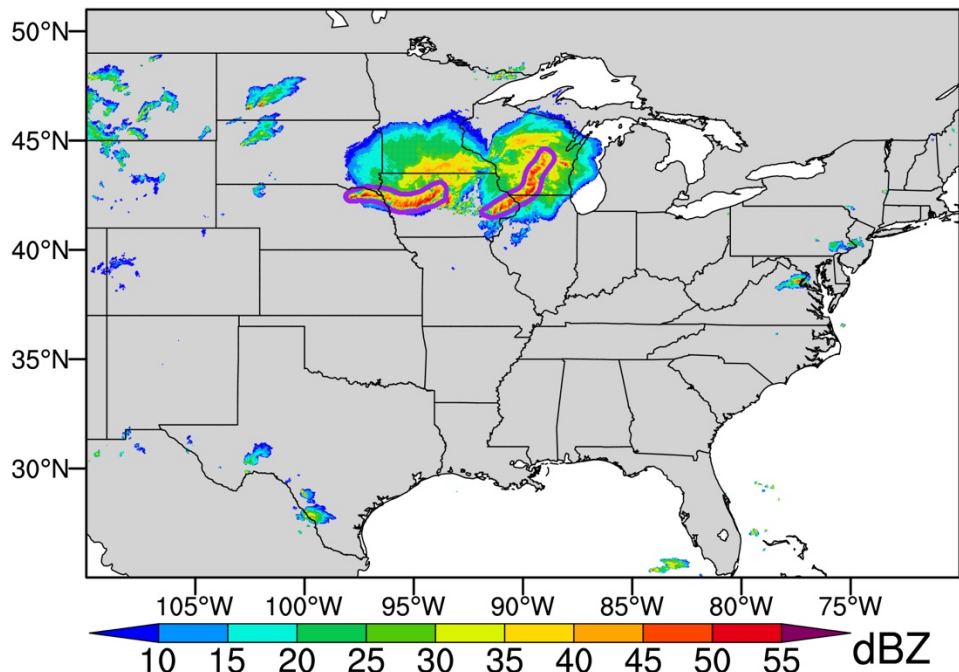
329
330   Figure 4. Examples of the U-Net 3+ CNN identified bow echoes (purple contours) based on Z_{Hmax} (color
331   shading) at 5:00 UTC on 17 June 2014.

332   Instead of validating our segmentation model at a pixel scale, as during the training stage, we prefer

333   evaluating its performance in detecting bulk bow echo features. In other words, we care about whether the

334   segmentation model can recognize the existence of bow echoes and capture their rough locations. Minor

335   spatial biases in bow echo coverage do not affect our below derecho identification much, which contains

336   various flexible criteria to minimize their impacts, such as the buffer zone within 100 km of bow echoes.

337   We also choose to validate the segmentation CNN specifically on MCS events where high reflectivity

338   features are present. Identifying low-reflectivity and echo-free images as non-bow echoes is desirable for

339   our segmentation model but trivial and not of particular interest for creating a derecho climatology.

340   To build a testing dataset, we randomly select 217 MCS-associated Z_{Hmax} images in 2010 based on

341   the following requirements. Each image is from a different MCS event. The images have variable sizes

342   and contain the full spatial extents of the MCSs at the selected times; however, they must be at least

343 192x192 pixels and cannot be drawn from a day that also has a sample in the training dataset. Three of the

344 authors independently assessed the presence of bow echoes in each image, the results of which are then

345 compared to the segmentation CNN (Table 1). Overall, the CNN model identifies 57 bow echoes, while

346 human labelers 1, 2, and 3 identify 46, 76, and 66, respectively. The average human-human agreement

347 and F_1 scores are 82% and 0.69, while the average human-CNN agreement and F_1 scores are 82% and

348 0.67 (Table 1). The test indicates that, on the one hand, the detection of bow echoes in radar images is

349 prone to subjective bias; on the other hand, the performance of the segmentation CNN is comparable to

350 that of a human in identifying bow echoes. We emphasize that the CNN bow echo identification is only

351 one component in our following derecho detection criteria, and the adverse impact of this uncertainty is

352 mitigated by other constraints (e.g., almost continuous bow echo existence and strong gusts in proximity

353 with bow echoes).

354 Table 1 Evaluation of the performance of the segmentation CNN in the bow echo identification[1]

	CNN (57[2])	Person 1 (46)	Person 2 (76)	Person 3 (66)
CNN		84%	79%	83%
Person 1	0.66		77%	88%
Person 2	0.66	0.59		81%
Person 3	0.70	0.77	0.70	

355 [1]The upper triangular part of the table shows agreement between two independent identifications
356 ($Agreement = \frac{TP+TN}{TP+TN+FP+FN}$), and the lower triangular part shows F_1 scores ($F_1 = \frac{2TP}{2TP+FP+FN}$), which is
357 a better indication of the ability to agree on positives when positives are a minority (Taha and Hanbury, 2015).
358 Here, TP denotes true positive, TN refers to true negative, FP is false positive, and FN is false negative.
359 Notably, for the comparison between any two independent identifications, we consider one as "true" and
360 evaluate the other against it (and which set of classifications is considered true does not impact these two
361 metrics).
362 [2]The number of identified bow echoes from the 217 images.

363 We match the segmentation CNN detected bow echoes with MCS events from the MCS dataset and

364 identify those MCS-associated bow echoes, which are used to identify derechos in the following section.

365 Figure 5 shows the spatial distribution of MCS-associated bow echo occurrences from 2004 to 2021,

366 which is similar to the MCS spatial distribution with more frequent occurrences in the Great Plains (Li et

367 al., 2021).
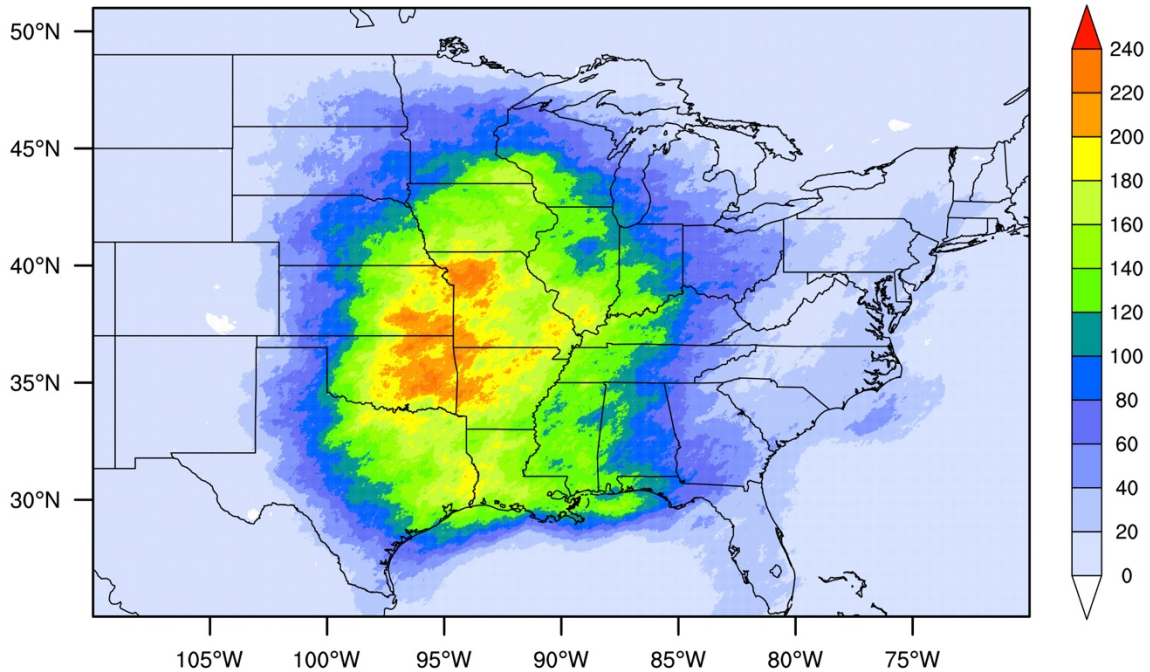
368
369 Figure 5. Spatial distribution of the number of MCS-associated bow echoes from 2004 to 2021. Here, we use
370 bow echo masks produced by the segmentation CNN and exclude bow echoes that do not overlap with MCS
371 events. This figure excludes bow echoes from those non-derecho-producing MCSs that overlap with tropical
372 cyclones (TCs) from the International Best Track Archive for Climate Stewardship (IBTrACS) Version 4 data
373 over the North Atlantic basin (Knapp et al., 2010) following the approach of Feng et al. (2021).

4 Derecho identification

4.1 Derecho definition

376   As mentioned above, we adopt the derecho definition proposed by Corfidi et al. (2016) but revise

377 certain criteria based on previous studies (Johns and Hirt, 1987; Bentley and Mote, 1998) and dataset

378 limitations to facilitate objective identification of derechos. Our final criteria are summarized below, with

379 detailed explanations provided afterward (Figure 6).

380   1)   A derecho must be attached to an MCS from the MCS dataset.

381   2)   The derecho must persist for at least 5 hours, with a bow echo present for at least 80% of its

382   lifetime. In addition, gaps between successive bow echo occurrences cannot exceed two hours.

383 All bow echoes must belong to the same bow echo series, as defined in the subsequent

384 explanation.

385 3) The derecho bow echo series must exhibit forward propagation, based on two modified criteria

386 from Corfidi et al. (2016):

387 • The acute angle between the averaged bow echo orientation and the bow echo series'

388 propagation direction must exceed 45° (Figure 6).

389 • The propagation speed of the bow echo series must be at least 30% greater than the

390 background mean wind speed at 500 hPa, derived from ERA5 data. The methodology

391 for calculating the averaged bow echo orientation, bow echo series' propagation

392 direction and speed, and the background mean wind speed is detailed in Appendix A.

393 4) Derecho-associated gust speed criteria vary based on the gust speed source dataset:

394 • For ISD data: Within 100 km of the derecho-accompanied bow echoes (termed the

395 "derecho area"), there must be at least 10 sites with strong gusts ($\geq$ 17.43 m s^{-1}) and at

396 least 1 site with damaging gusts ($\geq$ 25.93 m s^{-1}).

397 • For SED data: At least 10 locations must report damaging gusts.

398 • The fraction of sites with strong/damaging gusts (ISD) or damaging gusts (SED) must be

399 $\geq$ 20%.

400 • Gaps between successive strong (ISD) or damaging (SED) gust reports cannot exceed

401 two hours.

402 • The gust swath must be at least 650 km in length and 100 km in width. Swath length and

403 width calculations are explained below.

404
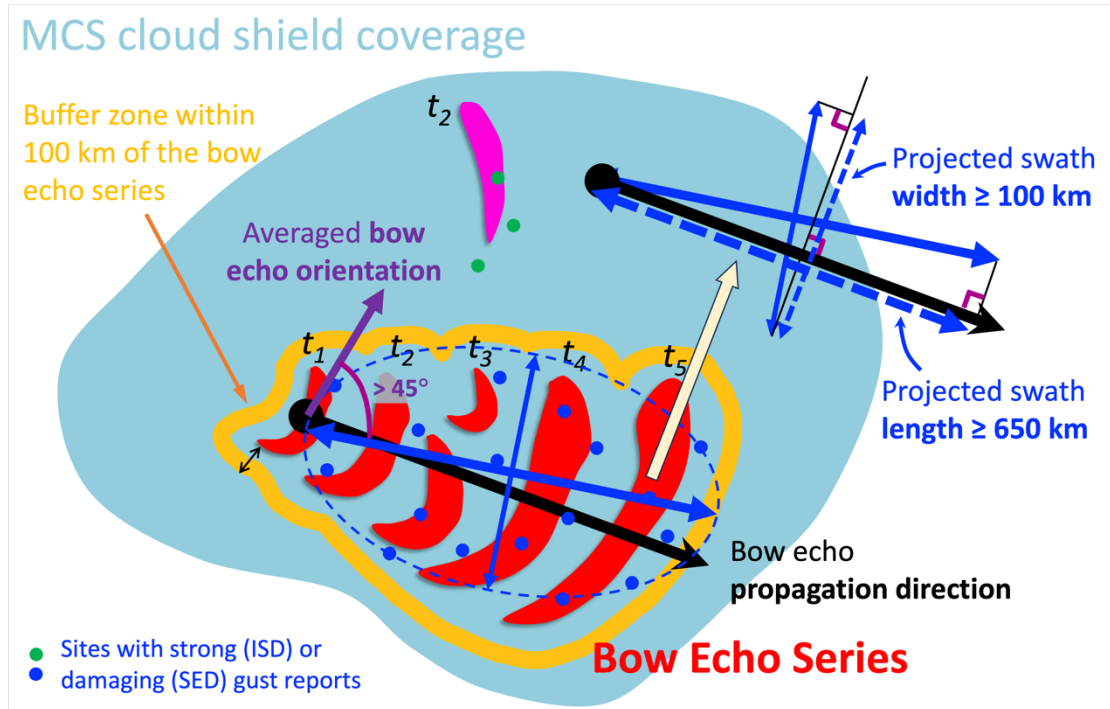
Figure 6. Schematic of the automated detection algorithm. Red and pink objects represent bow echoes. At time t_2, there are two bow echoes belonging to different bow echo series due to their great distance from each other. In contrast, the two bow echoes at t_3 are from the same bow echo series since they are close to each other. The pink bow echo at t_2 is far from the bow echoes at t_1 and t_3. Therefore, they belong to different bow echo series. The sites (green dots) with strong (for ISD) or damaging (for SED) gusts outside the 100-km buffer zone of the bow echo series (i.e., the derecho area) are excluded from the strong (ISD) or damaging (SED) gust swath calculation. The black arrow indicates the propagation direction of the bow echo series, and the violet arrow indicates the averaged bow echo orientation. Their acute angle must be > 45° for a derecho. The upper-right corner illustrates how the major and minor axis lengths of the gust fitted ellipse are projected onto another coordinate paralleling to the bow echo series' propagation direction to calculate gust swath length and width.

4.2 Explanation of Key Criteria and Adjustments

Criterion 1: MCS Association

This is a straightforward requirement and a major advantage of our approach. Due to the lack of a reliable MCS dataset, previous studies often spent considerable effort identifying spatiotemporally continuously propagating convective systems (Squitieri et al., 2023).

Criterion 2: Bow Echo Occurrence and Series Definition

422   The 80% bow echo occurrence threshold and the ≤ 2-hour lapse time between consecutive bow

423   echoes account for uncertainties in the segmentation CNN identification process and the diversity of MCS

424   events.

425   A bow echo series is defined in two steps:

426   1. Spatial grouping: Within a given MCS, bow echoes occurring in the same hour are categorized

427   into separate series if they are more than 100 km apart.

428   2. Temporal linking: Successive bow echoes (no more than 2 hours can elapse between their

429   occurrences) are considered part of the same series if they are less than 200 km apart, even if

430   they were initially classified as separate series.

431   Due to merging or splitting or the complex nature of some convective systems, a bow echo at one

432   hour may be far from the bow echoes right after or before that hour or another bow echo during that hour

433   (Figure 6). In such a rare situation, these bow echoes are unlikely caused by the same physical process

434   and, therefore, do not belong to the same bow echo series (Figure 6). The above stepwise approach

435   ensures that bow echoes from different physical processes are not incorrectly grouped.

436   Criterion 3: Forward Propagation Adjustment

437   We modify the Corfidi et al. (2016) criterion of "nearly orthogonal" to > 45° for the acute angle

438   between the averaged bow echo orientation and the bow echo series' propagation direction. This

439   adjustment:

440   •   Accounts for segmentation CNN uncertainties, particularly in the propagation direction

441   estimation.

442   •   Reduces false exclusions caused by minor variations in orientation.

443   Criterion 4: Gust Speed and Swath Calculation

444   The 20% fraction threshold is introduced to exclude MCSs potentially associated with extratropical

445   cyclones, which often produce isolated strong or damaging gusts but weaker gusts across most sites. It is

446   noteworthy that this criterion is primary applicable to ISD data, and its implementation for SED data

447   excludes only one MCS from being considered a potential DMCS.

448   To determine the gust swath length and width:

449   1. We fit an ellipse around sites with strong (ISD) or damaging (SED) gusts in the derecho area

450   (Figure 6).

451   2. Since the ellipse may not align with the bow echo series' propagation direction, we project its

452   major and minor axes onto a new coordinate system based on the bow echo propagation

453   direction, as shown on the upper right corner of Figure 6. The projected major or minor axis

454   length that is parallel to the bow echo propagation direction is the gust swath length, and the

455   projected minor or major axis length that is perpendicular to the propagation direction is the

456   swath width. Notably, both major and minor axis lengths can be projected parallelly and

457   perpendicularly. If major axis length is projected parallelly, the minor axis length must be

458   projected perpendicularly, and vice versa. Thus, we obtain two pairs of swath length and width.

459   3. We consider the uncertainties of the bow echo propagation direction when conducting the

460   projection. In detail, we conduct projections iteratively by varying the propagation direction

461   values with an interval of 0.2° within ±10° of the initial calculated bow echo series' propagation

462   direction. Therefore, we obtain $\left(\frac{20}{0.2} + 1\right) \times 2 = 202$ pairs of swath length and width in total.

463   As long as one pair of swath length and width satisfies length $\geq$ 650 km and width $\geq$ 100 km,

464   Criterion 4 is satisfied.

465   If no derecho is identified for a given MCS using the above definition criteria, we can relax the

466   distance requirement (100 km) in Criterion 4 to be within 200 km of the derecho-associated bow echoes

467   that satisfy the condition that there is no bow echo from the same bow echo series an hour ago or later

468   during the derecho's lifetime. If the bow echo is in the first hour of the derecho's lifetime and there are no

469   bow echoes for the corresponding MCS an hour ago, we can also extend the distance threshold to 200 km.

470   This is similar to the bow echo in the last hour of the derecho's lifecycle but without CNN-identified bow

471   echoes an hour later. Notably, the distance extension is optional. For the bow echoes satisfying the above

472   conditions, the distance threshold can be either 100 or 200 km. Using 100 km is superior to using 200 km

473   until we find a derecho if it exists. The distance extension is also intended to minimize the impacts of the

474   bow echo identification error. If a bow echo is missed in the semantic segmentation procedure, extending

475   the distance threshold can include strong and damaging gusts associated with the missed bow echo, thus

476   slightly reducing the derecho detection error.

477   We emphasize that, in Criterion 4, our ISD gust speed criteria are weaker than the SED gust speed

478   criteria as well as those of previous studies (Squitieri et al., 2023; Bentley and Mote, 1998; Johns and

479   Hirt, 1987), which also estimated the gust swath based on SED damaging gusts. As mentioned in Section

480   2.2.2, most SED gust reports are estimates, while ISD provides gust measurements from weather stations.

481   SED estimates can capture potential damaging gust occurrences over a much larger area, although with

482   large uncertainties. In contrast, due to the limited coverage of observational sites, real-time ISD

483   measurements may miss substantial damaging gust occurrences in nearby regions. Therefore, we lower

484   the gust speed criteria to capture potential derechos when using ISD measurements. It does not mean that

485   the ISD-based derechos are weaker than the SED-based ones or even not derechos, as elaborated in

486   Section 5.

4.3 Derecho detection results and postprocessing

488   Using ISD gust measurements, the objective detection algorithm identifies 245 derechos and

489   associated DMCSs between 2004 and 2021. A notable example is the June 2012 North American derecho

490   (Figure 7). Figure 7a displays the CNN-identified bow echoes of the DMCS, and Figure 7b shows the

491   derecho area and associated gust speeds. As expected, the derecho produced widespread strong gusts.

492   To further refine the ISD dataset, we manually review all detected derechos and DMCSs, removing

493   31 false detections due to erroneous bow echo identification (Figure S3). In addition, we examine 1099

494   MCS events that produce extensive strong ($\geq$ 10 observational sites) and damaging ($\geq$ 1) gusts over land

495   areas with a strong and damaging gust swath (fitted ellipse) of at least 650×100 km^2 (the ellipse's major

496   and minor axis lengths). Our manual examination primarily focuses on bow echo identification errors but

497   also slightly lower the forward propagating criteria thresholds for two potential derechos. For those MCSs

498   that are potential DMCSs based on our visual inspection, we manually label their bow echo occurrences

499   that fail the segmentation identification during potential derecho lifetimes (Figure S4) and rerun the

500   automated derecho detection algorithm. Finally, 60 additional derechos are added, bringing the final total

501   to 274 ($245 - 31 + 60 = 274$).

502   Using the same procedures for SED gust reports, we identify 220 derechos.

503
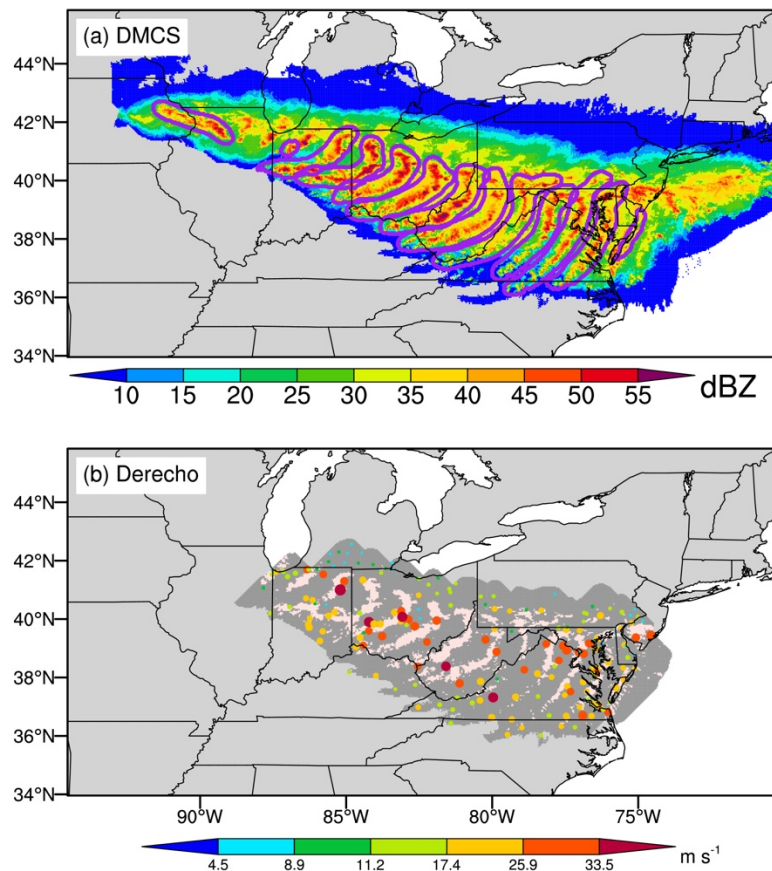
504 Figure 7. (a) Spatial evolution of Z_{Hmax} (color shading) and CNN-identified bow echoes (purple contours) from
505 the DMCS associated with the June 2012 North American derecho. (b) Similar to (a) but for the derecho
506 period. The derecho lasted from 17:00 UTC on 29 June to 6:00 UTC on 30 June 2012. The misty rose shading
507 in (b) corresponds to $Z_{Hmax} \geq 40$ dBZ, while the gray shading refers to the derecho area. Colored dots are the
508 same as those in Figure 1c, except only the derecho-associated gust measurements are shown.

5 Dataset evaluation and uncertainty

5.1 Evaluation against existing datasets

511   Between 2004 and 2021, our automated detection algorithm identifies 274 derechos (~ 15 per year)

512 using ISD gust measurements and 220 derechos (~12 per year) using SED gust reports-.. These numbers

513 fall within the range of previous estimations (6.1-20.9 per year) based on a 400 km swath length threshold

514 and conventional derecho definitions, as introduced in Section 1 (Squitieri et al., 2023; Johns and Hirt,

515 1987; Bentley and Mote, 1998; Evans and Doswell, 2001; Guastini and Bosart, 2016; Ashley and Mote,

516 2005). However,- our derecho counts are substantially higher than those reported by Corfidi et al. (2016),

517 who identified only 25 ~~derechos in the warm seasons of 2010-2014 using a 650 km swath length~~

518 ~~threshold. These discrepancies~~SED-based derechos in the warm seasons of 2010-2014 using a 650 km

519 swath length threshold. Our derecho numbers are also higher than those from Squitieri et al. (2025b), who

520 identified 70 SED-based derechos during 2000-2022 based on the physically-based definition criteria

521 from Corfidi et al. (2016) but with much stricter gust requirements (e.g., at least five reports of very

522 damaging gusts (≥ 33.53 m s^{-1})) for a 400-km-long gust swath (Squitieri et al., 2025a, b). The

523 discrepancies among the present study, Corfidi et al. (2016), and Squitieri et al. (2025b) could be

524 attributed to the different gust criteria used in the derecho definitions but also likely stem from differences

525 in the methods used to calculate gust swath length and width, the criteria for forward propagation, and the

526 diverse observational source datasets used in the derecho detection.

527   To further evaluate our dataset, we compare it against the NOAA Storm Prediction Center (SPC)

528 derecho data from 2004 and 2005 (https://www.spc.noaa.gov/misc/AbtDerechos/annualevents.htm; last

529 access: November 17, 2023) (Table 2). This dataset provides detailed timings and locations of derechos or

530 convective windstorms of near-derecho size, and it is the only available dataset that we can use to

531 evaluate our derecho dataset at the event scale. However, it is important to note that the NOAA SPC data

532 does not explicitly distinguish between derechos and convective windstorms of near-derecho size, and it

533 relies on the conventional derecho definition, which can significantly influence derecho counts.

534 Additionally, the NOAA SPC data is based on SED gust reports and lacks an underlying MCS database.

535   The NOAA SPC dataset contains 50 derechos and near-derecho size convective windstorms for 2004

536 and 2005, 15 of which are detected by our algorithm using ISD gust measurements. The number increases

537 to 19 when using SED gust reports. Five of the 50 events are entirely absent in our MCS dataset, possibly

538 because their associated MCSs moved too rapidly to satisfy PyFLEXTRKR's 50% areal overlap criterion

539 using hourly satellite and NEXRAD dataset, or they failed to meet other MCS requirements in

540 PyFLEXTRKR (Feng et al., 2019). The remaining discrepancies arise from factors such as an insufficient

541 number of damaging gust reports or bow echoes, too small a gust swath, or lack of forward propagation.

542 Conversely, our detection algorithm identifies several derechos (4 from ISD and 3 from SED) that are not

543 present in the NOAA SPC dataset. Overall, while most derechos identified by our algorithm are captured

544 in the NOAA SPC data, our derecho counts are notably lower due to our stricter physically-based derecho

545 definition, which reduces the number of events classified as derechos compared to conventional

546 definitions.

547   Cross validation between the ISD-based and SED-based datasets further supports the robustness of

548 our detection algorithm (Figure 8). A total of 172 derechos are detected by both datasets, while 48 events

549 are identified only in SED and 102 events are unique to ISD. Figure 8 also highlights discrepancies

550 between the two datasets, with more ISD-based than SED-based derechos in 2008, 2010, 2014, 2015,

551 2019, and 2020, while their counts remain similar in other years. Despite these differences, the two

552 datasets exhibit similar interannual variability, with a temporal correlation coefficient of 0.72. The general

553 agreement between the two datasets ~~support~~supports our decision to use different gust speed thresholds

554   for ISD and SED in the detection algorithm. However, the observed discrepancies also

555   ~~underscores~~underscore the critical role of the source datasets in influencing detection results, highlighting

556   the need for more reliable gust speed observations.
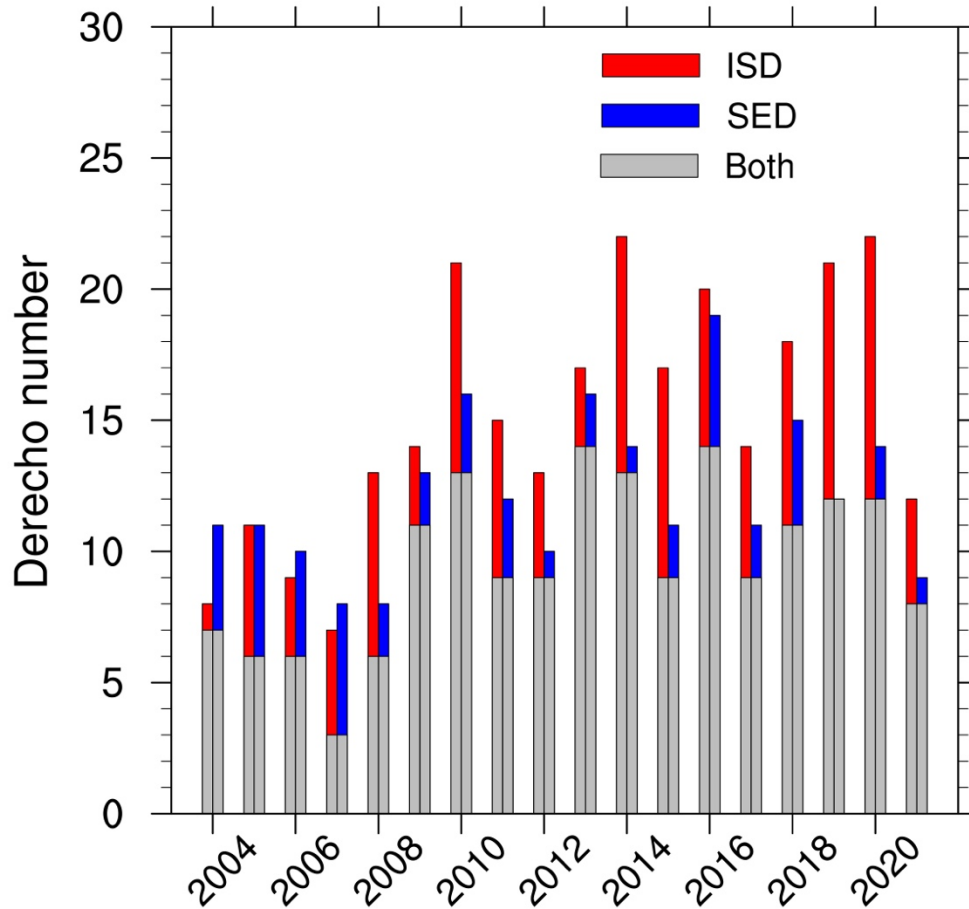
557
558   Figure 8. Bar chart of the annual derecho numbers from the ISD-based and the SED-based datasets from 2004
559   to 2021. Gray shading denotes derechos captured by both datasets, red shading refers to derechos only
560   identified when using ISD gust observations, and blue shading represents SED-only derechos.

561 **Table 2. Evaluation of our derecho dataset against the NOAA SPC data in 2004 and 2005**

	Year 2004	Year 2005	Sum
NOAA SPC	24	26	50
Captured by the ISD dataset	7	8	15
Captured by the SED dataset	10	9	19
Derechos in ISD but not in NOAA SPC	1	3	4
Derechos in SED but not in NOAA SPC	1	2	3
NOAA SPC events missed in the MCS dataset	2	3	5

562

5.2 Discussion on dataset uncertainty

Besides the uncertainties in gust speed observations, we acknowledge additional sources of uncertainty affecting our dataset.

5.2.1 Uncertainty from the MCS dataset

As noted in our evaluation against the NOAA SPC data, uncertainties arise from the MCS dataset used in derecho detection. The 50% areal overlap threshold in PyFLEXTRKR, which links consecutive cold cloud shields (CCSs), may fail to capture very fast-moving convective systems using hourly satellite and NEXRAD data. Lowering this threshold would undoubtedly increase the number of identified MCSs and derechos, but it could also introduce false tracks that do not belong to the same storm system. The 50% threshold is widely used in various versions of the FLEXTRKR algorithms (Li et al., 2021; Feng et al., 2023; Feng et al., 2019) and other tracking algorithms based on overlap (e.g., (Whitehall et al., 2015)). While we maintain this threshold in our study, users should be aware of uncertainties related to adjustable parameters (e.g., areal overlap threshold, MCS duration, and major axis length) and limitations in the observational datasets used by PyFLEXTRKR (Feng et al., 2019; Li et al., 2021).

5.2.2 Uncertainty from the bow echo identification

Another key uncertainty arises from the segmentation CNN used to identify bow echoes. While our evaluation in Section 3.3 confirms high accuracy, we acknowledge that some derechos may be missed, while some non-derechos may be falsely classified as derechos due to the bow echo identification errors. To mitigate this issue, we conducted extensive manual verification of derecho and DMCS events, as well as other MCS events producing widespread strong gusts. However, the manual examination introduces subjective biases, and completely eliminating bow echo identification uncertainties remains challenging.

584 *5.2.3 Uncertainty from derecho definition criteria*

585   Our detection algorithm relies on several adjustable parameters and methodological choices, all of

586 which influence the number of identified derechos. For example, to reduce the ISD-based derecho count

587 to the SED-based level, we must increase the ISD gust speed threshold in Criterion 4 in Section 4.1 from

588 17.43 m s^{-1} to 18.5 m s^{-1}; using the latter threshold produces a derecho number of 229, 152 of which

589 overlapped with the SED-based derecho dataset. While if we require at least ~~three~~five very damaging gust

590 reports (~~≥ 33.53 m s^{-1})~~ when using SED, the derecho count decreases substantially from 220 to ~~149.~~125,

591 which is still larger than but much closer to the estimates by Squitieri et al. (2025b) (70 derechos between

592 2000 and 2022). As the first climatological derecho dataset to incorporate bow echoes and provide

593 detailed event tracking, a full uncertainty assessment of all tunable parameters is beyond the scope of this

594 study. However, our sensitivity tests indicate that changes to key parameters (e.g., reducing the strong

595 gust fraction threshold to 10% or the number of sites with strong gust reports to 5) do not substantially

596 alter the derecho spatial distribution or seasonal variation patterns (see Section 6). Furthermore, our

597 dataset is designed to be flexible: we store all key parameters~~,~~ (e.g., gust swath length and width and bow

598 echo series' propagation speed), allowing users to apply stricter thresholds if needed to focus on stronger

599 derechos.

600   In summary, although our automated detection algorithm employs a physical-based derecho

601 definition rather than conventional definitions, our derecho counts are comparable to or slightly lower

602 than previous estimations, which is expected given our stricter criteria. Cross-validation between ISD-

603 based and SED-based datasets supports the high quality of our derecho dataset and the reliability of our

604 detection algorithm. However, users should be aware of the various sources of uncertainty in the dataset

605 generation, particularly those related to gust speed observations, MCS tracking criteria, bow echo

606 identification, and the choice of derecho definition parameters.

6 Derecho climatological characteristics

We primarily use the ISD-based derecho dataset to conduct the following climatological analyses, unless stated otherwise.

6.1 Annual statistics

Figure 8 displays the annual derecho numbers from 2004 to 2021. There is an apparent jump in the derecho number before (~10 derechos per year) and after 2007 (~15 derechos per year), which may be partially related to the general increase in the number of gust speed observational sites from 2004 to 2010 (Figure S5). Figure 9 shows the spatial distribution of yearly averaged annual ISD-based derecho numbers between 2004 and 2021. The central Great Plains has the most frequent derecho occurrences, extending to Oklahoma in the south, Iowa in the north, Kansas in the west, and Illinois in the east. The areas with frequent derecho occurrences are generally consistent with previous studies (Coniglio and Stensrud, 2004; Guastini and Bosart, 2016; Johns and Hirt, 1987; Ashley and Mote, 2005; Squitieri et al., 2025b), although some differences are identified. For example, several studies identified a remarkable northwest-southeast axis with frequent derecho occurrences extending from southern Minnesota to Ohio, which is observable but not apparent in our spatial distribution (Johns and Hirt, 1987; Coniglio and Stensrud, 2004; Guastini and Bosart, 2016; Squitieri et al., 2025b). The differences can be caused by many factors, such as distinct derecho definitions and observational datasets used in these studies. When we use SED gust reports in derecho detection, the spatial distribution of derecho counts shows a more noticeable northwest-southeast axis but with lower derecho numbers than the ISD-based dataset (Figure S6).
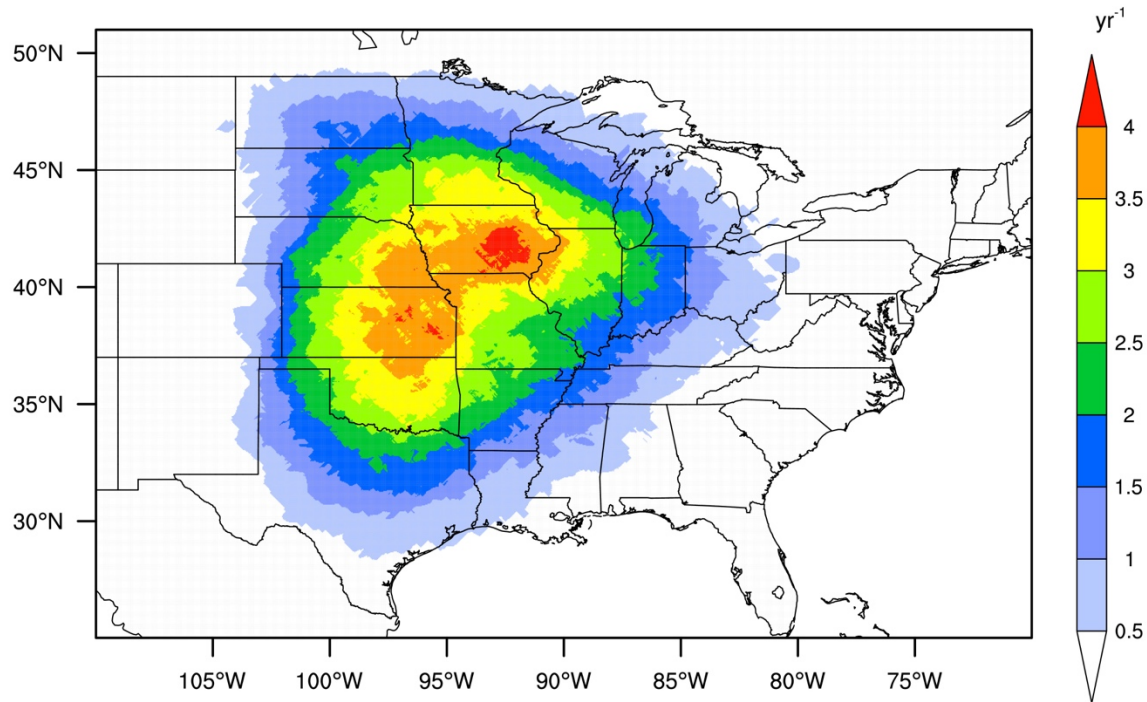
627
628 Figure 9. Spatial distribution of yearly averaged annual derecho numbers (ISD-based) over the United States
629 east of the Rocky Mountains between 2004 and 2021. Here, we use derecho areas as derecho spatial coverages.

6.2 Monthly statistics

631   Figure 10 displays the yearly averaged seasonal variations in the derecho count, with remarkably

632 more derechos in the warm than cold seasons, a feature consistent between ISD- and SED-based datasets

633 and widely captured by previous studies (Ashley and Mote, 2005; Squitieri et al., 2023; Squitieri et al.,

634 2025b; Bentley and Sparks, 2003). However, our dataset has almost no derechos in the ~~code season~~cold

635 seasons, which is generally not the case in previous studies~~.~~ except for Squitieri et al. (2025b), which also

636 used physically-based criteria to detect derechos. We thus attribute the ~~difference~~absence of cold-season

637 derechos to our usage of a physically-based derecho definition, which excludes many externally forced

638 convective systems (e.g., extratropical cyclones), which are considered serial derechos in previous

639 studies.

640   Figure 11 shows the spatial distributions of the monthly-mean derecho counts based on ISD between

641 2004 and 2021. On the one hand, many more derechos occur in the warm than cold months. On the other

642 hand, we find remarkable shifts in the areas with the most frequent derecho occurrences from April to

643 August. The region with the most derechos moves northward during the warm season. The northward

644 shifts resemble the MCS events (Li et al., 2021). We can identify two axes with frequent derecho

645 occurrences. One is in the south-north direction along the Great Plains (e.g., June), and the other is in the

646 west-east direction along the northern Great Plains and Midwest (e.g., July). ~~The axes may represent the~~

647 ~~two types (serial and progressive) of derechos mentioned in Squitieri et al. (2023). A follow-up study will~~

648 ~~be conducted to investigate the large-scale environmental conditions associated with different types of~~

649 ~~derechos based on the developed derecho dataset.~~The axes may represent two distinct types of

650 progressive derechos associated with different large-scale meteorological patterns. The SED-based dataset

651 shows similar features but with much fewer derechos in June (Figure S7).
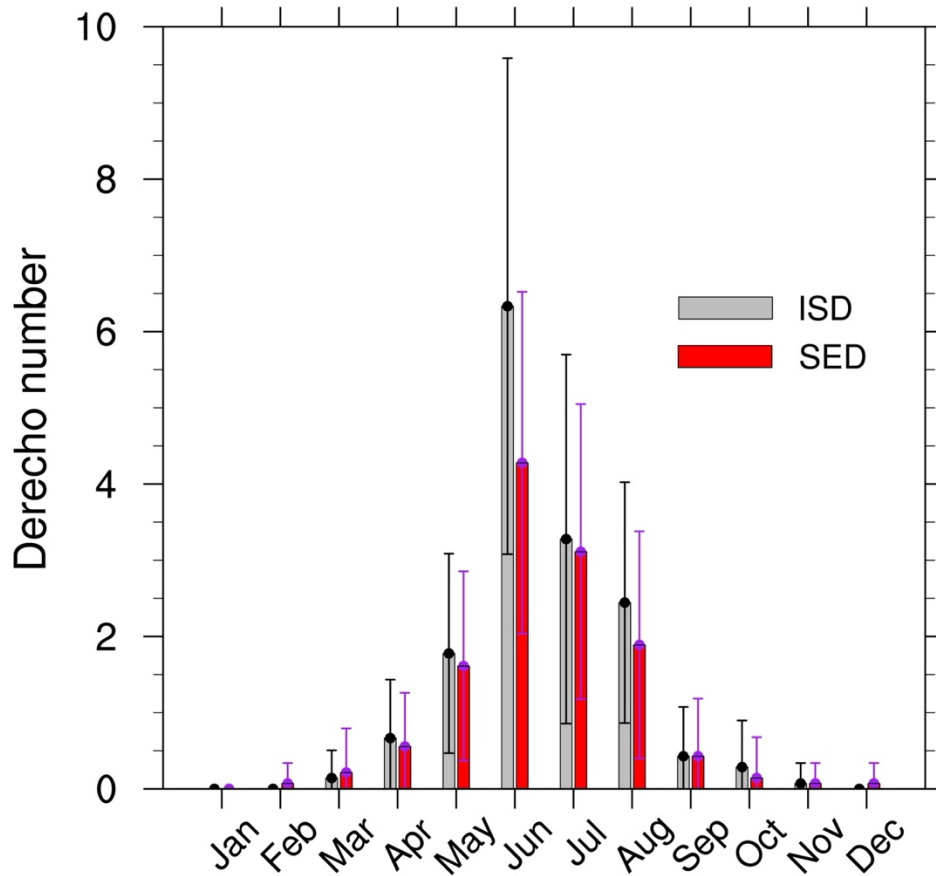
652
653 Figure 10. Yearly averaged monthly variations of the derecho numbers between 2004 and 2021. The error bars
654 denote standard deviations. Gray is for ISD-based derechos, and red colors indicate SED-based derechos.
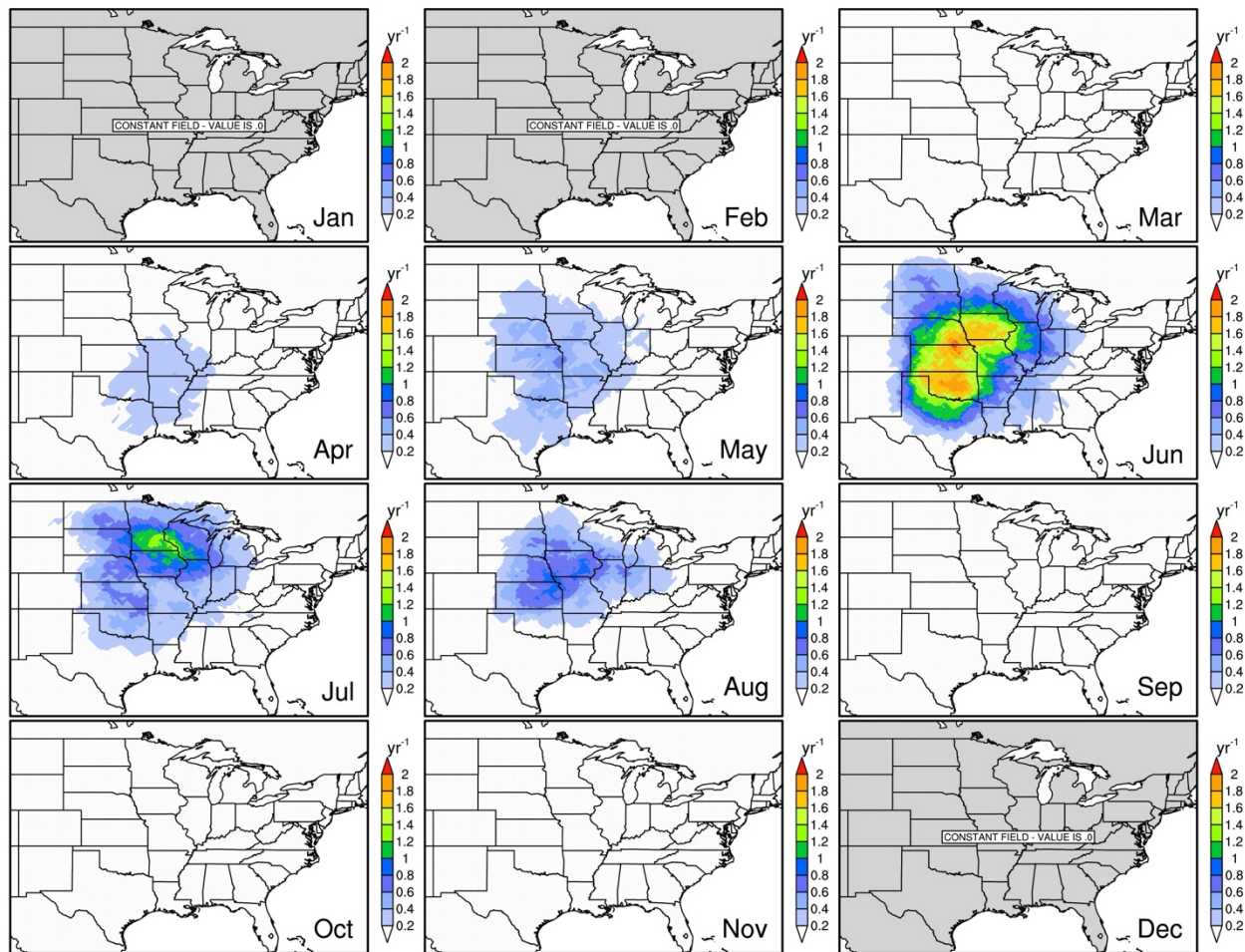
655
656 Figure 11. Same as Figure 9 but for yearly averaged monthly derecho numbers (ISD-based) over 2004-2021.

6.3 Wind damage characteristics

658   We examine the contributions of DMCSs and derechos to ISD damaging gust reports in the United

659 States within our dataset from 2004 to 2021 (Figures 12, S2, and S8). Notably, damaging gust reports

660 associated with a DMCS include those from the corresponding derecho as well as those falling outside the

661 derecho location or time window. Overall, MCSs contribute about 15.6% of all damaging gust reports,

662 with the vast majority occurring east of the Rocky Mountains. On average, DMCSs contribute 4.0%, and

663 derechos contribute 3.1% of all damaging gust occurrences. This indicates that about one quarter of the

664 damaging gusts associated with MCS events are linked to DMCSs, much higher than the fraction (~3.5%)

665 of DMCSs in MCSs. This finding aligns with the higher probabilities of extreme gusts in the gust speed

666 ~~PDF~~probability density function of DMCSs compared to general MCSs, indicating that DMCSs are more

667 likely to produce extreme gusts than general MCSs (Figure S9). Understanding the mechanisms behind

668 their contrast will be a key focus of a follow-up study. Additionally, approximately 75% of DMCS-

669 associated damaging gusts occur during the derecho period, reinforcing the validity of our derecho

670 definition. As expected, the highest contributions of derechos to damaging gust reports are found in the

671 Great Plains and Midwest (Figure 12).
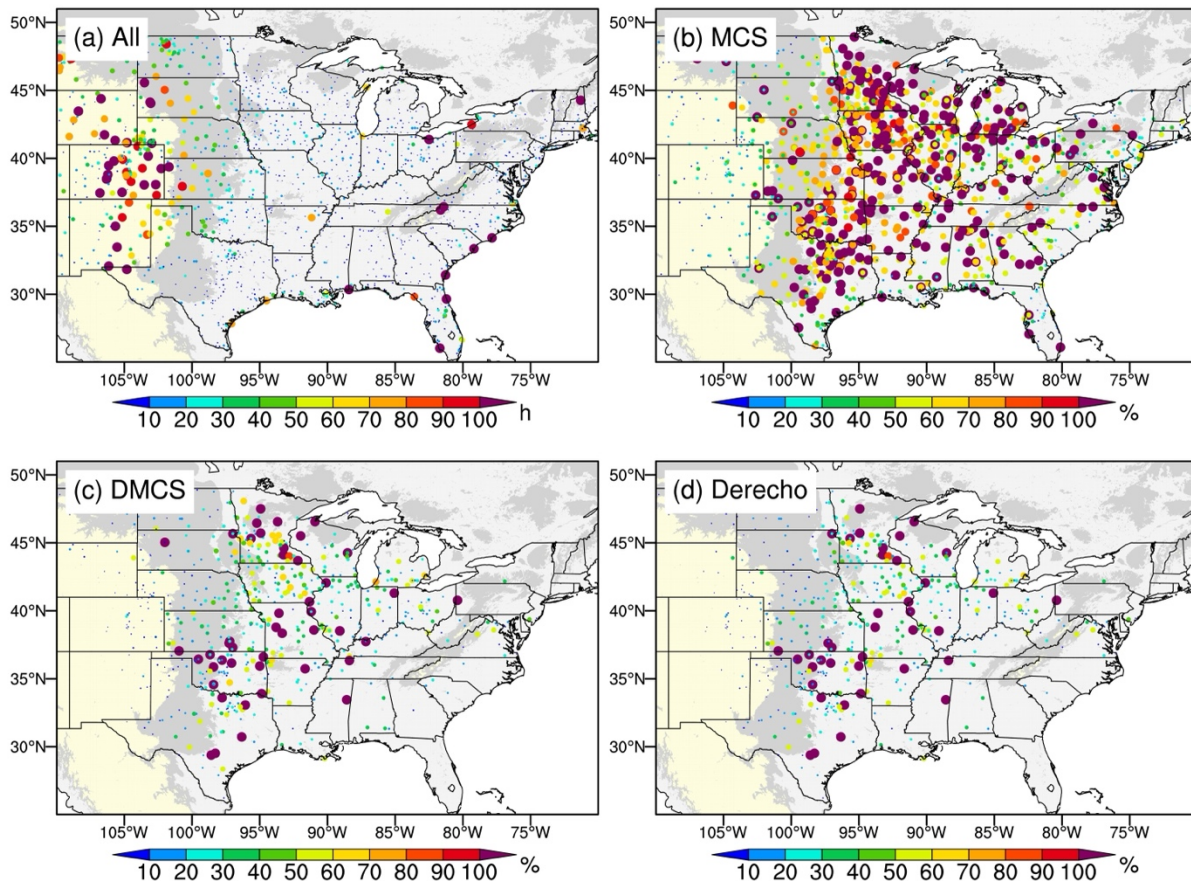
672
673 Figure 12. (a) The total numbers of damaging gust occurrences between 2004 and 2021 at ISD weather stations
674 over the United States east of the Rocky Mountains. (b) Relative contributions of MCS events to the damaging
675 gust occurrences in (a). (c) is the same as (b) but for relative contributions of DMCSs. (d) is the same as (c),
676 but for derechos. Similar to Figure 5, we exclude non-derecho-producing MCS events overlapping with TCs in
677 (b). The dot sizes are proportional to the corresponding values. Light-yellow shading denotes an elevation
678 greater than 1000 m; light-gray shading denotes an elevation between 400 m and 1000 m; and smoke-white
679 shading denotes an elevation less than 400 m. Background white is for oceans and lakes.

7 Data availability

The final ISD-based and SED-based derecho and DMCS dataset, along with the corresponding user guide, is publicly available at https://doi.org/10.5281/zenodo.14835362 (Li et al., 2025). The dataset is stored in NetCDF-4 format and compressed by year for easier access. The user guide provides a detailed description of the data files, ensuring that users can effectively navigate and utilize the dataset.

For each pair of derecho and DMCS, the dataset includes two visualization figures (one for derecho and the one for the accompanying DMCS) illustrating the temporal evolutions of Z_{Hmax}, precipitation, wind speed, and gust speed throughout their respective lifetimes (e.g., Figures 13 and S10). These figures offer users an immediate understanding of the basic characteristics of each derecho and DMCS. The dataset also contains all the derecho-associated gust speeds and various parameter values used in the derecho definition. This allows users to further categorize derechos by intensity or type, following approaches similar to Coniglio and Stensrud (2004).

For researchers interested in applying the segmentation CNN for bow echo detection in different regions or time periods, or in leveraging the CNN-identified bow echoes for other studies, we provide access to the bow echo segmentation code and datasets at https://doi.org/10.5281/zenodo.10822721 (Geiss et al., 2024). This repository includes the trained CNN weights and detailed usage instructions. Additionally, a video supplement demonstrating the bow echo segmentation scheme is available at https://youtu.be/iHWY_OhaVUo and is permanently archived in the above Zenodo repository.

20150602T20:00:00Z - 20150604T00:00:00Z
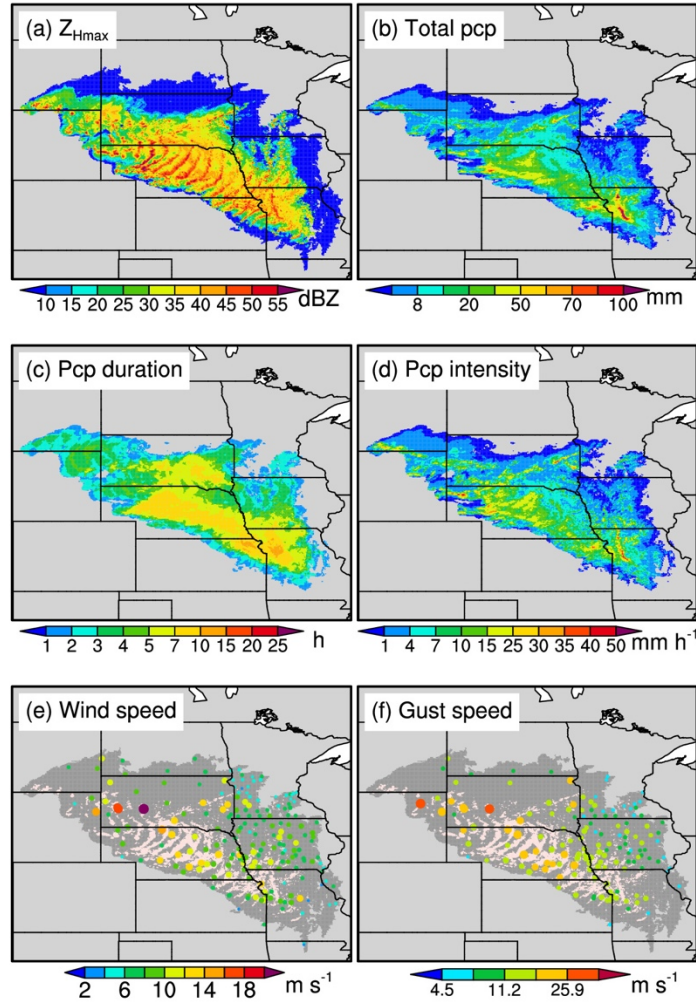
698
699 Figure 13. Similar to Figure 1 but for the spatial evolutions of (a) Z_{Hmax}, (b) total accumulated precipitation, (c)
700 precipitation duration, (d) mean precipitation intensity, (e) hourly maximum wind speed, and (f) hourly
701 maximum gust speed for a ISD-based DMCS that occurred on 2-4 June 2015. In (e) and (f), the misty rose
702 shading corresponds to areas with $Z_{Hmax} \geq 40$ dBZ, and the dark gray shading refers to DMCS coverage with
703 $Z_{Hmax} < 40$ dBZ. The figure title refers to the DMCS timing range.

8 Conclusions

705   This study presents a high-resolution (4 km and hourly) observational derecho dataset covering the

706 United States east of the Rocky Mountains from 2004 to 2021. We develop the dataset using a

707 combination of: an MCS dataset generated by the PyFLEXTRKR, bow echoes identified by a semantic

708 segmentation CNN, hourly gust speed data from ISD or SED, and physically based derecho identification

709 criteria.

710   • ~~An MCS dataset generated by the PyFLEXTRKR,~~

711   • ~~Bow echoes identified by a semantic segmentation CNN,~~

712   • ~~Hourly gust speed datasets from ISD or SED, and~~

713   • ~~Physically based derecho identification criteria.~~

714   We evaluate the dataset and its potential uncertainties. The final dataset identifies 274 derechos using

715 ISD gust measurements and 220 derechos using SED gust reports, with most events occurring in the

716 warm season (April-August). Analyses indicate that derechos preferentially occur in the Great Plains and

717 Midwest, with regions of highest frequency shifting northward from April to August. Derechos contribute

718 3.1% of ISD land-based damaging gusts over the United States between 2004 and 2021. Additionally,

719 approximately 20% of MCS-associated damaging gusts are produced by derechos.

720   As the first derecho dataset that integrates machine-learning-based bow echo identification,

721 physically based definition criteria, and two types of surface gust speed data, the dataset serves as an

722 independent reference for derecho climatology, complementing previous studies. Beyond climatological

723 analyses, the dataset can be used to~~:~~

724   • ~~Investigate~~ investigate the derecho initiation and development mechanisms,

725   • ~~Examine~~examine the environmental conditions that promote derecho formation and

726   intensification,

727   • ~~Assess~~assess the impacts of derechos on human safety and property, and

728   • ~~Select~~ select specific events for case studies or to evaluate the numerical model simulations,

729 thanks to its high spatiotemporal resolution.

730   Lastly, we emphasize that the automated derecho detection algorithm developed in this study is

731 versatile and applicable to both observations and model results. The algorithm can be used to assess

732 model performance and explore the impact of various factors on derechos (Kaminski et al., 2025).

Appendix A

733

734   For each bow echo in the derecho bow echo series, we use the formulas from the MATrix

735 LABoratory (MATLAB) "regionprops" function (https://github.com/SBU-

736 BMI/nscale/blob/master/original-matlab/features/regionprops.m; last access: January 28, 2025) to

737 calculate its orientation. Then we apply the three-sigma rule to the orientations to remove outliers until all

738 the rest orientations lie within three standard deviations of their mean. The mean is the average bow echo

739 orientation. Implementing the three-sigma rule aims to minimize the adverse impact of the segmentation

740 CNN identification uncertainties on calculating the averaged bow echo orientation.

741   The bow echo series' propagation direction and speed are calculated as follows. Firstly, we compute

742 the moving direction and speed between any two consecutive bow echoes from the series. As exemplified

743 in Figure A1, we assume that the bow echo at time t_1 would move to the location of bow echo t_1' at time t_2

744 if the bow echo shape remained unchanged. The location of bow echo t_1' is determined by its spatial

745 correlation coefficient with bow echo t_2, and the location with the largest spatial correlation coefficient is

746 what we want. Since bow echoes t_1 and t_1' have the same shape, it is straightforward to calculate the

747 moving direction and speed between them, which are considered the moving direction and speed between

748 bow echoes t_1 and t_2. Compared to using the centroid points of bow echoes t_1 and t_2, our approach can

749 reduce the calculation bias when bow echoes t_1 and t_2 have distinct shapes and sizes. After we obtain all

750 the moving directions and speeds between any two consecutive bow echoes, we apply the $1.5 \times$

751 Interquartile Range (IQR) rule to remove outliers, considering potential CNN bow echo identification

752 errors. Lastly, the median of the remaining moving speed values is considered the bow echo series'

753 propagation speed, while the average of the remaining move direction values is considered the bow echo

754 series' propagation direction.
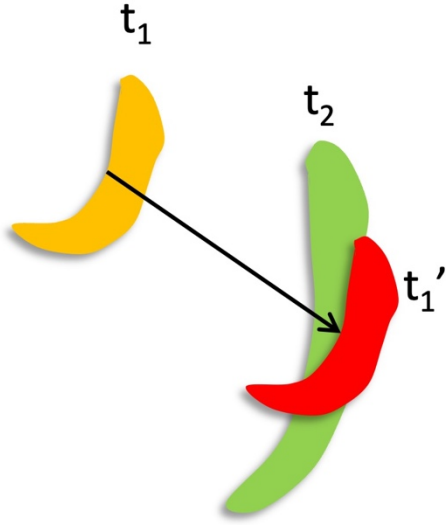
755
756 Figure A1. Schematic of the bow echo moving direction and speed calculation between two consecutive
757 (t_1 and t_2) bow echoes. Bow echo t_1' is the same as bow echo t_1 but at a different location so that the
758 spatial correlation coefficient between bow echoes t_1' and t_2 reaches the maximum. The moving direction
759 and speed between bow echoes t_1 and t_1' are considered the moving direction and speed between bow
760 echoes t_1 and t_2.

761   We use wind speeds at 500 hPa from ERA5 to compute the background mean wind speed.

762 Considering the potential spatiotemporal variability of 500-hPa winds, we only count wind speeds

763 covered by bow echoes from the bow echo series during the corresponding period. In detail, at time t_i

764 during the bow echo series period (t_1–t_n), we only consider winds at time t_i but covered by bow echoes

765 from time t_{i+1} to $min(t_{i+3}, t_n)$. Here, we exclude the bow echo at time t_i to minimize the potential impact

766 of the bow echo on the background environment, while using up to three hours (t_{i+1}–t_{i+3}) of bow echoes

767 aims to reduce the potential spatial noise since a bow echo is often too small. We average all wind speeds

768 obtained from the above procedure to derive the background mean wind speed.

Author Contributions

770 JL, ZF, and LRL designed the study. JL prepared the input files for PyFLEXTRKR, and ZF ran

771 PyFLEXTRKR to generate the MCS dataset. JL and ZF generated the initial positive and negative bow

772 echo samples. AG trained and validated the CNN model. AG applied the trained semantic segmentation

773 CNN to identify bow echoes from the MCS dataset with discussions with JL and ZF. JL defined and

774   identified derechos with discussions with ZF. JL evaluated the derecho dataset and manually examined

775   the data. JL analyzed the derecho climatology with discussions with ZF. JL wrote the manuscript except

776   for the machine-learning part which was written by AG. All co-authors reviewed the manuscript.

Competing Interests

778   The authors declare that they have no conflict of interest.

Acknowledgments

780   The NOAA SPC derechos and near-derechos are available at

781   https://www.spc.noaa.gov/misc/AbtDerechos/annualevents.htm (last access: November 17, 2023). The

782   named derechos we use to generate bow echo samples are from

783   https://en.wikipedia.org/wiki/List_of_derecho_events (last access: 19 March 2023). The elevation data is

784   from http://iridl.ldeo.columbia.edu/SOURCES/.NOAA/.NGDC/.GLOBE/ (last access: March 7, 2024).

785   The IBTrACS Version 4 TC data over the North Atlantic basin is from https://doi.org/10.25921/82ty-

786   9e16 (Knapp et al., 2018). Thank Drs. Israel L. Jirak, Brian J. Squitieri, and Andrew R. Wade from

787   NOAA SPC for discussing the derecho definition criteria with us.

Financial support

789   This research is supported by the Regional and Global Model Analysis and Multisector Dynamics

790   program areas of the U.S. Department of Energy Office of Science Biological and Environmental

791   Research as part of the HyperFACETS project. PNNL is operated for the Department of Energy by

792   Battelle Memorial Institute under Contract DE-AC05-76RL01830.

793

References

Adams-Selin, R. D. and Johnson, R. H.: Mesoscale surface pressure and temperature features associated with bow echoes, Monthly Weather Review, 138, 212-227, https://doi.org/10.1175/2009MWR2892.1, 2010.

Ardon-Dryer, K., Gill, T. E., and Tong, D. Q.: When a Dust Storm Is Not a Dust Storm: Reliability of Dust Records From the Storm Events Database and Implications for Geohealth Applications, GeoHealth, 7, e2022GH000699, https://doi.org/10.1029/2022GH000699, 2023.

Ashley, W. S. and Mote, T. L.: Derecho hazards in the United States, Bulletin of the American Meteorological Society, 86, 1577-1592, https://doi.org/10.1175/BAMS-86-11-1577, 2005.

Bardis, M., Houshyar, R., Chantaduly, C., Ushinsky, A., Glavis-Bloom, J., Shaver, M., Chow, D., Uchio, E., and Chang, P.: Deep learning with limited data: Organ segmentation performance by U-Net, Electronics, 9, 1199, https://doi.org/10.3390/electronics9081199, 2020.

Bentley, M. L. and Mote, T. L.: A climatology of derecho-producing mesoscale convective systems in the central and eastern United States, 1986–95. Part I: Temporal and spatial distribution, Bulletin of the American Meteorological Society, 79, 2527-2540, https://doi.org/10.1175/1520-0477(1998)079<2527:ACODPM>2.0.CO;2, 1998.

Bentley, M. L. and Sparks, J. A.: A 15 yr climatology of derecho-producing mesoscale convective systems over the central and eastern United States, Climate research, 24, 129-139, https://www.jstor.org/stable/24868368, 2003.

Bishop, C. M.: Pattern recognition and machine learning, Information Science and Statistics, 4, Springer, New York, NY, 2006.

Bowman, K. P. and Homeyer, C. R.: GridRad - Three-Dimensional Gridded NEXRAD WSR-88D Radar Data, the National Center for Atmospheric Research, Computational and Information Systems Laboratory [dataset], https://doi.org/10.5065/D6NK3CR7, 2017 (last access: 3 November 2022).

CDIACS/EOL/NCAR/UCAR and CPC/NCEP/NWS/NOAA: NCEP/CPC Four Kilometer Precipitation Set, Gauge and Radar, the National Center for Atmospheric Research, Computational and Information Systems Laboratory [dataset], https://doi.org/10.5065/D69Z93M3, 2000 (last access: 31 October 2022).

Coniglio, M. C. and Stensrud, D. J.: Interpreting the climatology of derechos, Weather and forecasting, 19, 595-605, https://doi.org/10.1175/1520-0434(2004)019<0595:ITCOD>2.0.CO;2, 2004.

Corfidi, S. F., Coniglio, M. C., Cohen, A. E., and Mead, C. M.: A proposed revision to the definition of "derecho", Bulletin of the American Meteorological Society, 97, 935-949, https://doi.org/10.1175/BAMS-D-14-00254.1, 2016.

Evans, J. S. and Doswell, C. A.: Examination of derecho environments using proximity soundings, Weather and Forecasting, 16, 329-342, https://doi.org/10.1175/1520-0434(2001)016<0329:EODEUP>2.0.CO;2, 2001.

Feng, Z.: Mesoscale convective system (MCS) database over United States (V3) [dataset], https://doi.org/10.5439/1571643, 2024 (last access: ~~25 Feburary~~7 February 2025).

Feng, Z., Hardin, J., Barnes, H. C., Li, J., Leung, L. R., Varble, A., and Zhang, Z.: PyFLEXTRKR: a flexible feature tracking Python software for convective cloud analysis, Geoscientific Model Development, 16, 2753-2776, https://doi.org/10.5194/gmd-16-2753-2023, 2023.

Feng, Z., Houze, R. A., Leung, L. R., Song, F., Hardin, J. C., Wang, J., Gustafson, W. I., and Homeyer, C. R.: Spatiotemporal characteristics and large-scale environments of mesoscale convective systems east of the Rocky Mountains, Journal of Climate, 32, 7303-7328, https://doi.org/10.1175/JCLI-D-19-0137.1, 2019.

Feng, Z., Leung, L. R., Liu, N., Wang, J., Houze Jr, R. A., Li, J., Hardin, J. C., Chen, D., and Guo, J.: A global high-resolution mesoscale convective system database using satellite-derived cloud tops, surface precipitation, and tracking, Journal of Geophysical Research: Atmospheres, 126, e2020JD034202, https://doi.org/10.1029/2020JD034202, 2021.

Fujita, T. T.: Proposed characterization of tornadoes and hurricanes by area and intensity, https://ntrs.nasa.gov/api/citations/19720008829/downloads/19720008829.pdf, 1971.

Galea, D., Ma, H.-Y., Wu, W.-Y., and Kobayashi, D.: Deep Learning Image Segmentation for Atmospheric Rivers, Artificial Intelligence for the Earth Systems, 3, 230048, https://doi.org/10.1175/AIES-D-23-0048.1, 2024.

Geiss, A. and Hardin, J. C.: Radar super resolution using a deep convolutional neural network, Journal of Atmospheric and Oceanic Technology, 37, 2197-2207, https://doi.org/10.1175/JTECH-D-20-0074.1, 2020.

Geiss, A., Li, J., Feng, Z., and Leung, L. R.: Bow echo detection and segmentation, Zenodo [dataset], https://doi.org/10.5281/zenodo.10822721, 2024 (last access: 15 March 2024).

Guastini, C. T. and Bosart, L. F.: Analysis of a progressive derecho climatology and associated formation environments, Monthly Weather Review, 144, 1363-1382, https://doi.org/10.1175/MWR-D-15-0256.1, 2016.

Hersbach, H., Bell, B., Berrisford, P., Biavati, G., Horányi, A., Muñoz Sabater, J., Nicolas, J., Peubey, C., Radu, R., Rozum, I., Schepers, D., Simmons, A., Soci, C., Dee, D., and Thépaut, J.-N.: ERA5 hourly data on single levels from 1940 to present, Copernicus Climate Change Service (C3S) Climate Data Store (CDS) [dataset], https://doi.org/10.24381/cds.adbb2d47, 2023 (last access: ~~1 November 2022~~3 June 2024).

Huang, G., Liu, Z., Pleiss, G., Van Der Maaten, L., and Weinberger, K. Q.: Convolutional networks with dense connectivity, IEEE transactions on pattern analysis and machine intelligence, 44, 8704-8716, https://doi.org/10.1109/TPAMI.2019.2918284, 2019.

Huang, H., Lin, L., Tong, R., Hu, H., Zhang, Q., Iwamoto, Y., Han, X., Chen, Y.-W., and Wu, J.: Unet 3+: A full-scale connected unet for medical image segmentation, ICASSP 2020-2020 IEEE international conference on acoustics, speech and signal processing (ICASSP), 1055-1059, https://doi.org/10.1109/ICASSP40776.2020.9053405, 2020.

867 Janowiak, J., Joyce, B., and Xie, P.: NCEP/CPC L3 Half Hourly 4km Global (60S - 60N) Merged IR V1,
868 Goddard Earth Sciences Data and Information Services Center (GES DISC) [dataset],
869 https://doi.org/10.5067/P4HZB9N27EKU, 2017 (last access: 27 September 2022).

870 Johns, R. H. and Hirt, W. D.: Derechos: Widespread convectively induced windstorms, Weather and
871 Forecasting, 2, 32-49, https://doi.org/10.1175/1520-0434(1987)002<0032:DWCIW>2.0.CO;2, 1987.

872 Kaminski, K., Ashley, W. S., Haberlie, A. M., and Gensini, V. A.: Future Derecho Potential in the United
873 States, Journal of Climate, 38, 3-26, https://doi.org/10.1175/JCLI-D-23-0633.1, 2025.

874 Ketkar, N.: Introduction to keras, Deep learning with Python: a hands-on introduction, 97-111,
875 https://doi.org/10.1007/978-1-4842-2766-4_7, 2017.

876 Kingma, D. P. and Ba, J.: Adam: A method for stochastic optimization, arXiv preprint arXiv:1412.6980,
877 https://doi.org/10.48550/arXiv.1412.6980, 2014.

878 Knapp, K. R., Diamond, H. J., Kossin, J. P., Kruk, M. C., and Schreck, C. J. I.: International Best Track
879 Archive for Climate Stewardship (IBTrACS) Project, Version 4, [North Atlantic], NOAA National
880 Centers for Environmental Information [dataset], https://doi.org/10.25921/82ty-9e16, 2018 (last access: 5
881 March 2024).

882 Knapp, K. R., Kruk, M. C., Levinson, D. H., Diamond, H. J., and Neumann, C. J.: The international best
883 track archive for climate stewardship (IBTrACS) unifying tropical cyclone data, Bulletin of the American
884 Meteorological Society, 91, 363-376, https://doi.org/10.1175/2009BAMS2755.1, 2010.

885 Kumler-Bonfanti, C., Stewart, J., Hall, D., and Govett, M.: Tropical and extratropical cyclone detection
886 using deep learning, Journal of Applied Meteorology and Climatology, 59, 1971-1985,
887 https://doi.org/10.1175/JAMC-D-20-0117.1, 2020.

888 Lagerquist, R., Turner, D., Ebert-Uphoff, I., Stewart, J., and Hagerty, V.: Using deep learning to emulate
889 and accelerate a radiative transfer model, Journal of Atmospheric and Oceanic Technology, 38, 1673-
890 1696, https://doi.org/10.1175/JTECH-D-21-0007.1, 2021.

891 Li, J., Feng, Z., Qian, Y., and Leung, L. R.: A high-resolution unified observational data product of
892 mesoscale convective systems and isolated deep convection in the United States for 2004–2017, Earth
893 Syst. Sci. Data, 13, 827-856, https://doi.org/10.5194/essd-13-827-2021, 2021.

894 Li, J., Geiss, A., Feng, Z., and Leung, L. R.: A derecho climatology over the United States from 2004 to
895 2021, Zenodo [dataset], https://doi.org/10.5281/zenodo.14835362, 2025 (last access: 78 February 2025).

896 Mounier, A., Raynaud, L., Rottner, L., Plu, M., Arbogast, P., Kreitz, M., Mignan, L., and Touzé, B.:
897 Detection of bow echoes in kilometer-scale forecasts using a convolutional neural network, Artificial
898 Intelligence for the Earth Systems, 1, e210010, https://doi.org/10.1175/AIES-D-21-0010.1, 2022.

899 NOAA/NCEI: Global Hourly - Integrated Surface Database (ISD), the National Oceanic and Atmospheric
900 Administration (NOAA) National Centers for Environmental Information (NCEI) [dataset],
901 https://www.ncei.noaa.gov/data/global-hourly/archive/isd/, 2001 (last access: 21 January 2023).

NOAA/NCEI: Federal Climate Complex Data Documentation For Integrated Surface Data (ISD), 126, https://www.ncei.noaa.gov/data/global-hourly/doc/isd-format-document.pdf, 2018.

NOAA/NCEI: Storm Events Database [dataset], https://www.ncdc.noaa.gov/stormevents/, 2025 (last access: 27 August 2024).

Ouali, Y., Hudelot, C., and Tami, M.: An overview of deep semi-supervised learning, arXiv preprint arXiv:2006.05278, https://doi.org/10.48550/arXiv.2006.05278, 2020.

Peláez-Vegas, A., Mesejo, P., and Luengo, J.: A Survey on Semi-Supervised Semantic Segmentation, arXiv preprint arXiv:2302.09899, https://doi.org/10.48550/arXiv.2302.09899, 2023.

Ronneberger, O., Fischer, P., and Brox, T.: U-net: Convolutional networks for biomedical image segmentation, Medical Image Computing and Computer-Assisted Intervention–MICCAI 2015: 18th International Conference, Munich, Germany, October 5-9, 2015, Proceedings, Part III 18, 234-241, https://doi.org/10.1007/978-3-319-24574-4_28,

Santos, R. P. d.: Some comments on the reliability of NOAA's Storm Events Database, arXiv preprint, https://doi.org/10.48550/arXiv.1606.06973, 2016.

Sha, Y., Gagne II, D. J., West, G., and Stull, R.: Deep-learning-based gridded downscaling of surface meteorological variables in complex terrain. Part I: Daily maximum and minimum 2-m temperature, Journal of Applied Meteorology and Climatology, 59, 2057-2073, https://doi.org/10.1175/JAMC-D-20-0057.1, 2020.

Smith, A., Lott, N., and Vose, R.: The integrated surface database: Recent developments and partnerships, Bulletin of the American Meteorological Society, 92, 704-708, https://doi.org/10.1175/2011BAMS3015.1, 2011.

Squitieri, B. J., Wade, A. R., and Jirak, I. L.: A historical overview on the science of derechos: part I: identification, climatology, and societal impacts, Bulletin of the American Meteorological Society, 104, E1709-E1733, https://doi.org/10.1175/BAMS-D-22-0217.1, 2023.

Squitieri, B. J., Wade, A. R. and Jirak, I. L.: On a modified definition of a derecho. Part I: Construction of the definition and quantitative criteria for identifying future derechos over the contiguous United States, Bulletin of the American Meteorological Society, 106(1), E84-E110, https://doi.org/10.1175/BAMS-D-24-0015.1, 2025a.

Squitieri, B. J., Wade, A. R. and Jirak, I. L.: On a modified definition of a derecho. Part II: An updated spatial climatology of derechos across the contiguous United States, Bulletin of the American Meteorological Society, 106(1), E111-E124, https://doi.org/10.1175/BAMS-D-24-0140.1, 2025b.

Starzec, M., Homeyer, C. R., and Mullendore, G. L.: Storm labeling in three dimensions (SL3D): A volumetric radar echo and dual-polarization updraft classification algorithm, Monthly Weather Review, 145, 1127-1145, https://doi.org/10.1175/MWR-D-16-0089.1, 2017.

Taha, A. A. and Hanbury, A.: Metrics for evaluating 3D medical image segmentation: analysis, selection, and tool, BMC medical imaging, 15, 1-28, https://doi.org/10.1186/s12880-015-0068-x, 2015.

938 Van Engelen, J. E. and Hoos, H. H.: A survey on semi-supervised learning, Machine learning, 109, 373-
939 440, https://doi.org/10.1007/s10994-019-05855-6, 2020.

940 Weisman, M. L.: The genesis of severe, long-lived bow echoes, Journal of the Atmospheric Sciences, 50,
941 645-670, https://doi.org/10.1175/1520-0469(1993)050<0645:TGOSLL>2.0.CO;2, 1993.

942 Weyn, J. A., Durran, D. R., Caruana, R., and Cresswell-Clay, N.: Sub-seasonal forecasting with a large
943 ensemble of deep-learning weather prediction models, Journal of Advances in Modeling Earth Systems,
944 13, e2021MS002502, https://doi.org/10.1029/2021MS002502, 2021.

945 White, C. H., Ebert-Uphoff, I., Haynes, J. M., and Noh, Y.-J.: Super-Resolution of GOES-16 ABI Bands
946 to a Common High Resolution with a Convolutional Neural Network, Artificial Intelligence for the Earth
947 Systems, https://doi.org/10.1175/AIES-D-23-0065.1, 2024.

948 Whitehall, K., Mattmann, C. A., Jenkins, G., Rwebangira, M., Demoz, B., Waliser, D., Kim, J., Goodale,
949 C., Hart, A., and Ramirez, P.: Exploring a graph theory based algorithm for automated identification and
950 characterization of large mesoscale convective systems in satellite datasets, Earth Science Informatics, 8,
951 663-675, https://doi.org/10.1007/s12145-014-0181-3, 2015.

952